Mathematical framework for Traction Force Microscopy

Richard Michel, Valentina Peschetola, Guido Vitale, Jocelyn Etienne, Alain Duperray, Davide Ambrosi, Luigi Preziosi, Claude Verdier

ESAIM: PROCEEDINGS, Vol. ?, 2013, 1-10
Editors: Will be set by the publisher

MATHEMATICAL FRAMEWORK FOR TRACTION FORCE MICROSCOPY

R. Michel [1], V. Peschetola [1,2], G. Vitale [3], J. Étienne [1], A. Duperray [4,5], D. Ambrosi [6], L. Preziosi [2] et C. Verdier [1]

Résumé. Cet article est consacré au problème de la *Microscopie à Force de Traction* (TFM). Ce problème consiste à déterminer les contraintes exercées par une cellule lors de sa migration sur un substrat élastique à partir d'une mesure expérimentale des déplacements induits dans ce substrat. Mathématiquement, il s'agit de résoudre un problème inverse pour lequel nous proposons une formulation abstraite de type optimisation sous contraintes. Les contraintes mathématiques expriment les constraintes biomécaniques que doit satisfaire le champ de contraintes exercé par la cellule. Ce cadre abstrait permet de retrouver deux des méthodes de résolution utilisées en pratique, à savoir la méthode adjointe (AM) et la méthode de Cytométrie de Traction par Transformée de Fourier (FTTC). Il permet aussi d'ameliorer la méthode FTTC. Les résultats numériques obtenus sont ensuite comparés et démontrent l'avantage de la méthode adjointe, en particulier par sa capacité à capturer des détails avec une meilleure précision.

Abstract. This paper deals with the *Traction Force Microscopy* (TFM) problem. It consists in obtaining stresses by solving an inverse problem in an elastic medium, from known experimentally measured displacements. In this article, the application is the determination of the stresses exerted by a living cell at the surface of an elastic gel. We propose an abstract framework which formulates this inverse problem as a constrained minimization one. The mathematical constraints express the biomechanical conditions that the stress field must satisfy. From this framework, two methods currently used can be derived, the adjoint method (AM) and the Fourier Transform Traction Cytometry (FTTC) method. An improvement of the FTTC method is also derived using this framework. The numerical results are compared and show the advantage of the AM, in particular its ability to capture details more accurately.

Key words. Cell motility, Inverse problems, Tikhonov regularization, Adjoint Method (AM), Fourier Transform Traction Cytometry (FTTC), L–curve.

[1] CNRS / Univ. Grenoble 1, Laboratoire Interdisciplinaire de Physique, UMR 5588, Grenoble, F-38041, France.
[2] Dipartimento di Matematica, Politecnico di Torino, 10129 Torino, Italy.
[3] Laboratoire de Mécanique des Solides, CNRS UMR 7649, École Polytechnique, 91128 Palaiseau Cedex, France.
[4] INSERM U823, Grenoble, France.
[5] Univ. Grenoble 1, Institut Albert Bonniot et Institut Français du sang, UMR-S823, Grenoble, France.
[6] MOX - Dipartimento di Matematica, Politecnico di Milano, Milano, Italy.

1. Introduction

Living cells have the ability to migrate on different 2D–susbstrates which are considered to be *in vitro* model for understanding cell motility. Indeed, cells pull on the substrate and can deform it by developing forces, which are called traction forces. It is essential to determine such forces, because one can then understand how cells regulate their adhesion and modify their cytoskeleton [4] in order to produce such a complex process, i.e. migration. To determine traction forces or more precisely traction stresses, assuming that cells do not penetrate into the substrate, biophysicists have proposed to use *beads* embedded in the substrate [11]. By following the positions of beads, as compared to their initial state, one obtains displacements in the migration plane. These displacements are denoted by $\boldsymbol{u}_\mathrm{b}$ and are defined on a part Ω_b of the whole computational domain (see Fig. 1 below). They are related to the stresses applied by cells by the elasticity problem. So, the determination of the traction stress field from the (partial) knowledge $\boldsymbol{u}_\mathrm{b}$ of the induced displacements needs to solve an *inverse elasticity problem*. This method has been called *Traction Force Microscopy (TFM)* and has been considered using different formulations, the BEM (Boundary Element Method (BEM) [11], the Fourier Transform Traction Cytometry (FTTC) method [8], the Traction Recovery from Point Force (TRPF) [22], and finally the more recent Adjoint Method (AM) [2,3,25].

An important point, sometimes neglected in the literature, is the fact that the traction stress field must satisfy a set of *biomechanical constraints*. First, the cell is not in contact with the substrate on the whole computational domain, but only over a subdomain denoted by Ω_c and called the *cell domain* (see Fig. 1 below). Therefore

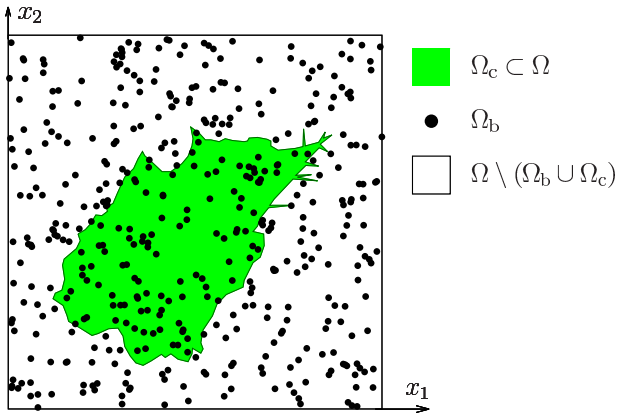

Figure 1. Schematic representation of the computational domain. Ω : 2D computational domain corresponding to the cell migration plane ; Ω_c : cell domain, the part of Ω "below" the cell ; Ω_b : beads domain. See also Fig. 2 page 10.

stresses are zero outside this cell domain. Next, if the cell moves slowly (as is the case) or in a quasistatic way, it is in equilibrium and the sum of forces and moments vanish. This can be written in mathematical terms as :

$$\mathrm{supp}\,(\boldsymbol{T}) \subset \overline{\Omega_\mathrm{c}}, \quad \int_{\Omega_\mathrm{c}} \boldsymbol{T}\,\mathrm{d}\boldsymbol{x} = 0 \quad \text{and} \quad \int_{\Omega_\mathrm{c}} \boldsymbol{x} \wedge \boldsymbol{T}\,\mathrm{d}\boldsymbol{x} = 0 \tag{1}$$

where $\boldsymbol{T}$ is the traction stress field exerted by cells on the substrate, $\overline{\Omega_\mathrm{c}}$ is the closure of Ω_c, and $\mathrm{supp}\,(\boldsymbol{T})$ is the support of $\boldsymbol{T}$, that is the complement of the largest set where $\boldsymbol{T}$ is identically zero almost everywhere. The three biomechanical conditions defined in (1) will be respectively called *localization constraint*, *zero force constraint*, and *zero moment constraint*.

After the seminal paper of Dembo *et al.* [11] the FTTC method [8] has been proposed as a simpler framework and more efficient in terms of computational time. Nevertheless, the FTTC method does not allow to impose the zero moment constraint and needs to be modified to account for one of the biomechanical conditions, the localization constraint which imposes no stresses outside the cell domain. A way to impose this localization constraint, called constrained–FTTC, has been proposed [8], but, to the best of our knowledge, it seems that this variant has never been used. In this work, we focus on the localization condition and we propose an improvement of the classical FTTC method to satisfy this constraint.

By contrast, the adjoint method does not have any difficulty to impose the biomechanical constraints (1). The localization constraint was imposed in [2], then the zero force constraint was taken into account [20]. More recently [25], the zero moment constraint was also imposed. This method could be thought of as a tool to differentiate different cells, in particular cancer cells with different invasiveness [2, 3, 19].

The outline of this paper is as follows. In the next section, we present an abstract variational framework which allows to formulate the TFM problem as a constrained minimization problem. In order to insure uniqueness and regularity of the solution, a regularization term is added to the objective function. This framework is used in section 3 to derive the adjoint method and in section 4 to improve the FTTC method in order to meet the localization constraint. In section 5, the issue of the choice of the regularization parameter is discussed and the traction stresses fields obtained by using adjoint method and improved FTTC method are compared in a real case.

2. Abstract variational framework for the TFM problem

In this section we define an abstract variational framework to formulate and solve the TFM problem. The functional framework is described in section 2.1 in terms of spaces and operators. Then, in section 2.2, we define the unknown traction stress field as the solution of a constrained minimization problem. Next, in section 2.3 we reformulate the optimal conditions as a set of unconstrained variational equations involving the adjoint state and the displacement field as unknowns. The traction stress field is then obtained by using a projection operator. Finally, in section 2.4 we summarize some classical results concerning the convergence of the regularization process.

2.1. **Functional framework**

Spaces. Let H be a real Hilbert space. We denote by $(\cdot,\cdot)_H$ its scalar product and by $||\cdot||_H = \sqrt{(\cdot,\cdot)_H}$ the corresponding norm. Let $V \subset H$ be a linear subspace of H. We assume that V is dense in H for the topology induced by the norm $||\cdot||_H$ ($\overline{V}^H = H$), and that, equipped with its own norm $||\cdot||_V$, V is a reflexive Banach space such that the injection from V into H is continuous ($V \hookrightarrow H$). Under these conditions, the canonical injection from the space H into its dual H' defines a linear continuous injective operator whose range is dense in H' [7]. If, by using the Riesz theorem, we identify H with its dual H' ($H \equiv H'$, that is H is chosen as *pivot space* for the duality pairing), then the spaces V, H and V' form a *Gelfand triple* :

$$V \hookrightarrow H \equiv H' \hookrightarrow V' \quad \text{with} \qquad \overline{V}^H = H \ \text{ and } \ \overline{H'}^{V'} = V' \tag{2}$$

Furthermore, the duality pairing satisfies the following relations

$$\langle \boldsymbol{T}, \boldsymbol{S} \rangle_{H',H} = (\boldsymbol{T}, \boldsymbol{S})_H \ \forall\ (\boldsymbol{T}, \boldsymbol{S}) \in H \times H \quad \text{and} \quad \langle \boldsymbol{T}, \boldsymbol{v} \rangle_{V',V} = (\boldsymbol{T}, \boldsymbol{v})_H \ \forall\ (\boldsymbol{T}, \boldsymbol{v}) \in H \times V \tag{3}$$

In the TFM context, V and H are respectively displacement and stress spaces and the injection of V into H is also compact. To take into account biomechanical constraints (1) and experimental data, we need two supplementary

spaces. The first one is H_c a closed non empty subspace of H related to biomechanical constraints, (or at least some of these constraints), and the second one is X_b, another real Hilbert space related to the experimentally measured displacements $\boldsymbol{u}_b$. Depending on the used formulation and on the nature of $\boldsymbol{u}_b$, X_b is either a finite dimensional space (see the section 4.4, or the formulation used in [25]), either a closed non empty subspace of H (when $\boldsymbol{u}_b$ is a function and Ω_b an open set). In both cases, we denote by $(\cdot,\cdot)_{X_b}$ and $||\cdot||_{X_b}$ the scalar product and its associated norm in X_b. Note that under these conditions, the space X_b can be identified with its dual space without contravening with the choice of the space H as pivot space.

Elasticity operator. The relationship between the stress field $\boldsymbol{T}$ imposed by the cell during its migration and the displacement $\boldsymbol{u}$ induced in the gel (on the gel surface) is represented by a continuous linear operator $A \in \mathscr{L}(V, V')$ from V into its dual V'. We assume the A is V-elliptic in the sense that :

$$\exists\, \alpha > 0 \text{ such that } \langle A\boldsymbol{v}, \boldsymbol{v}\rangle_{V',V} \geq \alpha\, ||\boldsymbol{v}||_V^2 \quad \forall\, \boldsymbol{v} \in V \tag{4}$$

Under these conditions, A is bijective. Furthermore, since V and V' are two Banach spaces, thanks to Banach theorem, the inverse A^{-1} is a linear continuous operator from V' into V. Thus, $A \in \mathit{Isom}(V, V')$ and $A^{-1} \in \mathit{Isom}(V', V)$. Hence, all stress fields $\boldsymbol{T}$ imposed by the cell and the induced displacements $\boldsymbol{u}$ in the gel are related by :

$$A\boldsymbol{u} = \boldsymbol{T} \text{ in } V' \quad \Longleftrightarrow \quad \boldsymbol{u} = A^{-1}\boldsymbol{T} \text{ in } V \tag{5}$$

In addition, the adjoint operator A^{T} is also an isomorphism and, thanks to reflexivity of V, we have $A^{\mathsf{T}} \in \mathit{Isom}(V, V')$ and $A^{-\mathsf{T}} \in \mathit{Isom}(V, V')$ where $A^{-\mathsf{T}}$ denotes the inverse of A^{T}.

Observation operator and data. To compare the theoretical displacements $\boldsymbol{u} = A^{-1}\boldsymbol{T} \in V$ to the *experimental beads displacements* $\boldsymbol{u}_b \in X_b$ we use a continuous linear operator $B \in \mathscr{L}(V, X_b)$ which can be viewed as the *observation* operator. This comparison involves the *residual vector* $BA^{-1}\boldsymbol{T} - \boldsymbol{u}_b \in X_b$. As X_b can be identified with its dual, we have $B^{\mathsf{T}} \in \mathscr{L}(X_b, V')$.

2.2. The TFM problem as a constrained minimization problem

Tikhonov functional. Given a positive real-valued parameter $\varepsilon > 0$, we define the so–called *Tikhonov functional* $J_\varepsilon : \boldsymbol{T} \in H \longmapsto J_\varepsilon(\boldsymbol{T}) \in \mathbb{R}^+$ by

$$J_\varepsilon(\boldsymbol{T}) = \frac{1}{2}\, \left|\left|BA^{-1}\boldsymbol{T} - \boldsymbol{u}_b\right|\right|_{X_b}^2 + \frac{\varepsilon}{2}\, ||\boldsymbol{T}||_H^2 \tag{6}$$

The following two propositions establish the differentiability and convexity properties that are needed.

Proposition 2.1 (**Differentiability**). *The Tikhonov functional $J_\varepsilon(\cdot)$ defined by* (6) *is twice Frechet–differentiable everywhere in H and, for all $\boldsymbol{T} \in H$, its first and second derivatives $J'_\varepsilon(\boldsymbol{T}) \in H'$ and $J''_\varepsilon(\boldsymbol{T}) \in \mathscr{L}(H \times H, \mathbb{R})$ read*

$$\langle J'_\varepsilon(\boldsymbol{T}), \boldsymbol{\delta T}\rangle_{H',H} \;=\; \left(BA^{-1}\boldsymbol{T} - \boldsymbol{u}_b, BA^{-1}\boldsymbol{\delta T}\right)_{X_b} \;+\; \varepsilon\, (\boldsymbol{T}, \boldsymbol{\delta T})_H \tag{7}$$

$$\langle J''_\varepsilon(\boldsymbol{T}), (\boldsymbol{\delta T}, \boldsymbol{\delta S})\rangle_{H',H} \;=\; \left(BA^{-1}\boldsymbol{\delta T}, BA^{-1}\boldsymbol{\delta S}\right)_{X_b} \;+\; \varepsilon\, (\boldsymbol{\delta T}, \boldsymbol{\delta S})_H \tag{8}$$

for all $(\boldsymbol{\delta T}, \boldsymbol{\delta S}) \in H \times H$.

Démonstration. Direct computation and application of the Frechet derivative definition. □

Proposition 2.2 (**Convexity**). *The Tikhonov functional $J_\varepsilon(\cdot)$ defined by* (6) *is strictly convex everywhere in H.*

Démonstration. From equation (8), we have $\langle J''_\varepsilon(\boldsymbol{T}), (\boldsymbol{\delta T}, \boldsymbol{\delta T})\rangle_{H',H} = \left|\left|BA^{-1}\boldsymbol{\delta T}\right|\right|^2_{X_\mathrm{b}} + \varepsilon \, ||\boldsymbol{\delta T}||^2_H \geq \varepsilon \, ||\boldsymbol{\delta T}||^2_H$ for all $\boldsymbol{\delta T} \in H$. So, since $\varepsilon > 0$, $J''_\varepsilon(\boldsymbol{T})$ is H–elliptic for all $\boldsymbol{T} \in H$. Then, the Tikhonov functional J_ε is strictly convex everywhere over H [10]. □

Now, we can define rigorously the required stress field $\boldsymbol{T}_\varepsilon$ as the solution of the following constrained minimization problem.

Problème 2.3. (**Constrained minimization problem**) Given $\boldsymbol{u}_\mathrm{b} \in X_\mathrm{b}$, and $\varepsilon > 0$, find $\boldsymbol{T}_\varepsilon$ such that

$$\boldsymbol{T}_\varepsilon \in H_\mathrm{c} \quad \text{and} \quad J_\varepsilon(\boldsymbol{T}_\varepsilon) = \min_{\boldsymbol{T}\in H_\mathrm{c}} J_\varepsilon(\boldsymbol{T}) \tag{9}$$

This problem is well-posed in the sense that the following theorem holds.

Théorème 2.4. *The constrained minimization problem 2.3 has one and only one solution $\boldsymbol{T}_\varepsilon$ which satisfies the following variational equation*

$$\boldsymbol{T}_\varepsilon \in H_\mathrm{c} \quad \textit{and} \quad \left(BA^{-1}\boldsymbol{T}_\varepsilon - \boldsymbol{u}_\mathrm{b}, BA^{-1}\boldsymbol{T}\right)_{X_\mathrm{b}} + \varepsilon \, (\boldsymbol{T}_\varepsilon, \boldsymbol{T})_H = 0 \quad \forall \boldsymbol{T} \in H_\mathrm{c} \tag{10}$$

Démonstration. The Tikhonov functional J_ε is strictly convex everywhere in H (cf. prop. 2.2), and H_c is a closed subspace of the Hilbert space H, so [7, 10], the minimization problem 2.3 has one and only one solution $\boldsymbol{T}_\varepsilon \in H_\mathrm{c}$. Moreover [7, 10], this solution satisfies the Euler equation $\langle J'_\varepsilon(\boldsymbol{T}_\varepsilon), \boldsymbol{T}\rangle_{H',H} = 0 \; \forall \boldsymbol{T} \in H_\mathrm{c}$ which, by using definition (7) of $J'_\varepsilon(\boldsymbol{T}_\varepsilon)$, is rewritten as (10). □

The definition (6) of the Tikhonov functional $J_\varepsilon(\cdot)$ involves two terms. The first one, the residual norm $\left|\left|BA^{-1}\boldsymbol{T} - \boldsymbol{u}_\mathrm{b}\right|\right|^2_{X_\mathrm{b}}$, measures the goodness of the optimal solution $\boldsymbol{T}_\varepsilon$, i.e. its ability to predict the experimental displacements $\boldsymbol{u}_\mathrm{b}$. Qualitatively, if this term is too large, $\boldsymbol{T}_\varepsilon$ cannot be considered as a suitable solution. But a small value is not necessarily a satisfying condition to meet. Indeed, when a small value of the residual norm occurs, then uncertainties in the data $\boldsymbol{u}_\mathrm{b}$ take too much weight. As a result, the solution $\boldsymbol{T}_\varepsilon$ is dominated by high–frequency components with large amplitudes and becomes so irregular that it looses its physical meaning. It is the well known instability of the inverse problem solution [14, 16]. So, the second term in the definition of $J_\varepsilon(\cdot)$, the stress norm $||\boldsymbol{T}||^2_H$, measures the regularity of the optimal solution $\boldsymbol{T}_\varepsilon$. Its role is to restore and enforce the stability of $\boldsymbol{T}_\varepsilon$ by penalizing its norm. The Tikhonov functional can be understood as a balance between two contradictory requirements : obtaining small residuals with a sufficiently smooth solution. The *regularization parameter* ε can be viewed as a tuning parameter for this balance. Large values of ε lead to very smooth stress fields with poor residuals. Conversely, smaller values of ε give good residuals with unrealistic stresses. In section 5, we deal with the manner to choose this regularization parameter.

Another way to regularize the TFM problem is to apply a low-pass filtering in order to avoid the high-frequency components in the experimental beads displacements [24].

The formulation of the TFM problem as the constrained minimization problem 2.3 is mathematically rigorous and is, in our opinion, a fundamental basis of any numerical methods for computing an approximation of stresses exerted by the cell. But this formulation is exclusively focused on the minimization aspects and does not address more specific aspects related to the inverse nature of the TFM problem. On this matter, we refer to recent work [25].

2.3. **Solving the TFM problem**

Adjoint state. By using the definition of the adjoint operator and the property (3) of the duality pairing, we can reformulate the $X_{\rm b}$–scalar product involved in the variational equation (10) as follows

$$\begin{aligned}\left(BA^{-1}\boldsymbol{T}_\varepsilon-\boldsymbol{u}_{\rm b},BA^{-1}\boldsymbol{T}\right)_{X_{\rm b}} &= \left\langle B^{\mathsf T}\left(BA^{-1}\boldsymbol{T}_\varepsilon-\boldsymbol{u}_{\rm b}\right),A^{-1}\boldsymbol{T}\right\rangle_{V',V}\\ &= \left\langle A^{-\mathsf T}B^{\mathsf T}\left(BA^{-1}\boldsymbol{T}_\varepsilon-\boldsymbol{u}_{\rm b}\right),\boldsymbol{T}\right\rangle_{V,V'}\\ &= \left(A^{-\mathsf T}B^{\mathsf T}\left(BA^{-1}\boldsymbol{T}_\varepsilon-\boldsymbol{u}_{\rm b}\right),\boldsymbol{T}\right)_H\end{aligned}$$

Note that this derivation uses explicitely the identification of the space $X_{\rm b}$ with its dual $X_{\rm b}'$.

By substituting this last identity in the variational equation (10), we obtain another equivalent characterization of the optimal stress field $\boldsymbol{T}_\varepsilon$

$$\boldsymbol{T}_\varepsilon\in H_{\rm c}\quad\text{ and }\quad\left(A^{-\mathsf T}B^{\mathsf T}\left(BA^{-1}\boldsymbol{T}_\varepsilon-\boldsymbol{u}_{\rm b}\right),\boldsymbol{T}\right)_H\;+\;\varepsilon\,(\boldsymbol{T}_\varepsilon,\boldsymbol{T})_H\;=\;0\quad\forall\boldsymbol{T}\in H_{\rm c}\tag{11}$$

Since $B^{\mathsf T}\in\mathscr{L}(X_{\rm b},V')$, $B^{\mathsf T}\left(BA^{-1}\boldsymbol{T}_\varepsilon-\boldsymbol{u}_{\rm b}\right)$ belongs to V', and $A^{\mathsf T}\in\mathscr{L}(V,V')$ is an isomorphism from V into its dual V', there exists one and only one element $\boldsymbol{p}_\varepsilon$ such that

$$\boldsymbol{p}_\varepsilon\in V\quad\text{ and }\quad A^{\mathsf T}\boldsymbol{p}_\varepsilon=B^{\mathsf T}\left(BA^{-1}\boldsymbol{T}_\varepsilon-\boldsymbol{u}_{\rm b}\right)\quad\text{ in }\quad V'\tag{12}$$

This field $\boldsymbol{p}_\varepsilon\in V$ is the classical *adjoint state* [18] applied to the TFM problem.

Interpretation of the optimal condition and projection operator. The adjoint state $\boldsymbol{p}_\varepsilon$ can be viewed as a simple auxiliary unknown which allows us to rephrase the characterization equation (11) of $\boldsymbol{T}_\varepsilon$. Indeed, by substituting the adjoint equation (12) into (11) we obtain

$$\boldsymbol{T}_\varepsilon\in H_{\rm c},\quad\boldsymbol{p}_\varepsilon\in V\quad\text{ and }\quad(\boldsymbol{p}_\varepsilon+\varepsilon\,\boldsymbol{T}_\varepsilon,\boldsymbol{T})_H\;=\;0\quad\forall\boldsymbol{T}\in H_{\rm c}\tag{13}$$

This new variational equation is nothing but the characterization of $-\varepsilon\,\boldsymbol{T}_\varepsilon\in H_{\rm c}$ as the *projection* of the adjoint state $\boldsymbol{p}_\varepsilon\in V$ (as an element of H) onto the biomechanical constraints space $H_{\rm c}$ [7,10], that is :

$$\boldsymbol{T}_\varepsilon\;=\;-\frac{1}{\varepsilon}\,P_{\rm c}\,\boldsymbol{p}_\varepsilon\quad\text{ in }H\tag{14}$$

where $P_{\rm c}$ is the projection operator from H onto $H_{\rm c}$ with respect to the scalar product $(\cdot,\cdot)_H$. Since $H_{\rm c}$ is a linear subspace of H, $P_{\rm c}$ is a linear continuous operator from H into H ($P_{\rm c}\in\mathscr{L}(H,H)$), furthermore, $P_{\rm c}$ is self–adjoint ($P_{\rm c}^{\mathsf T}=P_{\rm c}$) and idempotent ($P_{\rm c}\,P_{\rm c}=P_{\rm c}$).

Three fields problem. As $\boldsymbol{T}_\varepsilon\in H$, by using the injection $H\hookrightarrow V'$ involved by the Gelfand triple (2), $\boldsymbol{T}_\varepsilon$ also belongs to V'. So we can define the displacement field $\boldsymbol{u}_\varepsilon$ related to the stress field $\boldsymbol{T}_\varepsilon$ and defined as the solution of

$$\boldsymbol{u}_\varepsilon\in V\quad\text{ and }\quad A\,\boldsymbol{u}_\varepsilon=\boldsymbol{T}_\varepsilon\quad\text{ in }V'\tag{15}$$

Obviously, existence and uniqueness follow from $A\in Isom\,(V,V')$. Next, by substituting $\boldsymbol{T}_\varepsilon$ for $A\boldsymbol{u}_\varepsilon$ we can rewrite the adjoint equation (12) as

$$\boldsymbol{p}_\varepsilon\in V\quad\text{ and }\quad A^{\mathsf T}\boldsymbol{p}_\varepsilon=B^{\mathsf T}\left(B\boldsymbol{u}_\varepsilon-\boldsymbol{u}_{\rm b}\right)\quad\text{ in }\quad V'$$

On the other hand, by taking into acount (14) we reformulate (15) as a relationship between $\boldsymbol{u}_\varepsilon$ and $\boldsymbol{p}_\varepsilon$

$$\boldsymbol{u}_\varepsilon\in V\quad\text{ and }\quad A\,\boldsymbol{u}_\varepsilon=-\frac{1}{\varepsilon}P_{\rm c}\boldsymbol{p}_\varepsilon\quad\text{ in }V'\tag{16}$$

The previous discussion can be summarized by the following problem.

Problème 2.5. (**Three fields problem**) Given $\boldsymbol{u}_{\mathrm{b}} \in X_{\mathrm{b}}$ and $\varepsilon > 0$, find $(\boldsymbol{p}_\varepsilon, \boldsymbol{u}_\varepsilon, \boldsymbol{T}_\varepsilon) \in V \times V \times H_{\mathrm{c}}$ such that

1. $(\boldsymbol{p}_\varepsilon, \boldsymbol{u}_\varepsilon) \in V \times V$ is the solution of

$$\begin{array}{rcrcll} \dfrac{1}{\varepsilon} P_{\mathrm{c}}\, \boldsymbol{p}_\varepsilon & + & A\, \boldsymbol{u}_\varepsilon & = & 0 & \text{in } V' \\ A^{\mathsf{T}} \boldsymbol{p}_\varepsilon & - & B^{\mathsf{T}} B\, \boldsymbol{u}_\varepsilon & = & -B^{\mathsf{T}} \boldsymbol{u}_{\mathrm{b}} & \text{in } V' \end{array} \tag{17a, 17b}$$

2. then, deduce $\boldsymbol{T}_\varepsilon \in H_{\mathrm{c}}$ by

$$\boldsymbol{T}_\varepsilon = -\frac{1}{\varepsilon} P_{\mathrm{c}}\, \boldsymbol{p}_\varepsilon \quad \text{in } H \tag{17c}$$

This problem is well–posed and allows to solve the constrained minimization problem 2.3 as proved by the following theorem.

Théorème 2.6. *The three fields problem 2.5 has one and only one solution. Furthermore, the component $\boldsymbol{T}_\varepsilon$ of this solution is also the solution of the constrained minimization problem 2.3.*

Démonstration. Existence. The theorem 2.4 establishes the existence of $\boldsymbol{T}_\varepsilon \in H_{\mathrm{c}}$ which solves the constrained minimization problem 2.3. So, starting from this existence result for $\boldsymbol{T}_\varepsilon$, we can reproduce integrally the above discussion to establish the existence of a solution $(\boldsymbol{p}_\varepsilon, \boldsymbol{u}_\varepsilon, \boldsymbol{T}_\varepsilon) \in V \times V \times H_{\mathrm{c}}$ of the problem 2.5 such that its component $\boldsymbol{T}_\varepsilon$ solves the problem 2.3.

Uniqueness. Since the equations (17) are linear, to show uniqueness of their solution it is sufficient to show that the only solution of (17) corresponding to $\boldsymbol{u}_{\mathrm{b}} = 0$ is $(\boldsymbol{p}_\varepsilon, \boldsymbol{u}_\varepsilon, \boldsymbol{T}_\varepsilon) = (0, 0, 0)$. So, let $(\boldsymbol{p}_\varepsilon, \boldsymbol{u}_\varepsilon, \boldsymbol{T}_\varepsilon) \in V \times V \times H_{\mathrm{c}}$ be a solution of equations (17) corresponding to $\boldsymbol{u}_{\mathrm{b}} = 0$. If $\boldsymbol{u}_{\mathrm{b}} = 0$, since $A^{\mathsf{T}} \in \mathit{Isom}\,(V, V')$, equation (17b) yields $\boldsymbol{p}_\varepsilon = A^{-\mathsf{T}} B^{\mathsf{T}} B \boldsymbol{u}_\varepsilon$. Thus, equation (17c) can be rewritten as

$$P_{\mathrm{c}}\, A^{-\mathsf{T}} B^{\mathsf{T}} B \boldsymbol{u}_\varepsilon \; + \; \varepsilon\, A \boldsymbol{u}_\varepsilon \; = \; 0$$

By definition of the projection operator P_{c} (from H onto H_{c} in the sense of $(\cdot,\cdot)_H$) and because H_{c} is a linear space, we deduce that

$$\left(A^{-\mathsf{T}} B^{\mathsf{T}} B \boldsymbol{u}_\varepsilon \; + \; \varepsilon\, A \boldsymbol{u}_\varepsilon, \boldsymbol{T}\right)_H = 0 \;\; \forall\, \boldsymbol{T} \in H_{\mathrm{c}} \qquad \text{and} \qquad A\, \boldsymbol{u}_\varepsilon \in H_{\mathrm{c}}$$

Thus, we can choose $\boldsymbol{T} = A\, \boldsymbol{u}_\varepsilon$ in the previous variational equation and obtain

$$\left(A^{-\mathsf{T}} B^{\mathsf{T}} B \boldsymbol{u}_\varepsilon \; + \; \varepsilon\, A \boldsymbol{u}_\varepsilon, A\, \boldsymbol{u}_\varepsilon\right)_H \; = \; 0$$

By applying the definition of the adjoint operators A^{T} and B^{T}, this last equation leads to

$$||B\, \boldsymbol{u}_\varepsilon||^2_{X_{\mathrm{b}}} + \varepsilon \; ||A\, \boldsymbol{u}_\varepsilon||^2_H \; = \; 0$$

Since $\varepsilon > 0$, it then follows that $A\, \boldsymbol{u}_\varepsilon = 0$ in H. So $(A\boldsymbol{u}_\varepsilon, \boldsymbol{T})_H = 0$ for all $\boldsymbol{T} \in H$, and since $V \hookrightarrow H$, in particular holds for $\boldsymbol{T} = \boldsymbol{u}_\varepsilon$. According to (3) we have $(A\boldsymbol{u}_\varepsilon, \boldsymbol{u}_\varepsilon)_H = \langle A\boldsymbol{u}_\varepsilon, \boldsymbol{u}_\varepsilon \rangle_{V',V}$ and the V–ellipticity (4) of the operator A then gives $\boldsymbol{u}_\varepsilon = 0$. From equation (17b) written with $\boldsymbol{u}_{\mathrm{b}} = 0$, and since $A^{\mathsf{T}} \in \mathit{Isom}\,(V, V')$, we deduce that $\boldsymbol{p}_\varepsilon = 0$. As $P_{\mathrm{c}} \in \mathscr{L}\,(H, H)$, it follows from (17c) that $\boldsymbol{T}_\varepsilon = 0$. This ends the proof. □

The problem 2.5 and the theorem 2.6 provide a general framework where the Tikhonov method is used to solve the inverse TFM problem. A specific problem is essentially the choice of an operator A and a constraint space H_{c} in equations (17). The choices corresponding to the adjoint and FTTC methods are discussed in the next sections.

Remarque 2.7. When the projection operator P_{c} is explicitely known, equations (17) can be directly used to define a numerical method to approximate the optimal solution $\boldsymbol{T}_\varepsilon$. Indeed, under these conditions equations (17a) and (17b) a explicitely define an unconstrained problem and then the $\boldsymbol{p}_\varepsilon$–component of its solution can be explicitely calculated by using the projection step (17c). This situation occurs when only the localization constraint and the zero force constraint are imposed in the constrained space [20] (see (24) and (25) in the next section). This is precisely the situation in which the adjoint and FTTC methods can be compared.

When the zero moment constraint is also taken into acount, the projection operator P_{c} exists but not in an explicit form. So, the problem 2.5 remains only a theoretical one. To obtain a theoretical formulation which can produce a numerical method, it is better to impose the zero moment constraint by duality [25] using a Lagrange multiplier.

2.4. **Convergence propertries**

In this section, we consider the behavior of the family $(\boldsymbol{T}_\varepsilon)_{\varepsilon>0}$ of Tikhonov solutions when the regularization parameter ε varies. This section is a concise account of classical results [12,16]. More recent and specific results can be found for instance in [6].

In practice, experimental bead displacements $\boldsymbol{u}_{\mathrm{b}} \in X_{\mathrm{b}}$ are never known exactly. They are only an approximation of the exact bead displacements $\boldsymbol{u}_{\mathrm{b,exact}} \in X_{\mathrm{b}}$ and there exists a *noise level* $\delta > 0$ such that

$$||\boldsymbol{u}_{\mathrm{b}} - \boldsymbol{u}_{\mathrm{b,exact}}||_H \leq \delta \tag{18}$$

For instance, the uncertainly on the experimental data used in section 5 allows us to estimate the noise level around 0.03 µm for displacements of a few micrometers. This noise level δ plays a crucial role in the convergence of the familly $(\boldsymbol{T}_\varepsilon)_{\varepsilon>0}$ as $\varepsilon \longrightarrow 0$.

A first consequence of the presence of noise in the experimental data is that, in general, we cannot assume that the bead displacements $\boldsymbol{u}_{\mathrm{b}}$ are in the range $\mathcal{R}\left(BA^{-1}\right)$ of the operator BA^{-1}. Moreover, the observation operator B is not injective. Hence, in order to analyse the convergence properties of the familly $(\boldsymbol{T}_\varepsilon)_{\varepsilon>0}$, it is convenient to introduce the *Moore–Penrose generalized inverse* $\left(BA^{-1}\right)^+$ of BA^{-1} [12] and to define the so-called *best-approximate solution* $\boldsymbol{T}^+$ as the field

$$\boldsymbol{T}^+ = \left(BA^{-1}\right)^+ \boldsymbol{u}_{\mathrm{b,exact}} = AB^+ \boldsymbol{u}_{\mathrm{b,exact}}$$

where B^+ denotes the Moore–Penrose generalized inverse of the observation operator B.

Let us define the regularized solution $\boldsymbol{T}_{\varepsilon,\mathrm{exact}}$ related to the exact bead displacements as

$$\boldsymbol{T}_{\varepsilon,\mathrm{exact}} \in H_{\mathrm{c}} \quad \text{and} \quad J_{\varepsilon,\mathrm{exact}}(\boldsymbol{T}_{\varepsilon,\mathrm{exact}}) = \min_{\boldsymbol{T}\in H_{\mathrm{c}}} J_{\varepsilon,\mathrm{exact}}(\boldsymbol{T})$$

where the functional $J_{\varepsilon,\mathrm{exact}}(\cdot)$ is defined in the same manner than the Tikhonov functional (6) with $\boldsymbol{u}_{\mathrm{b,exact}}$ in place of $\boldsymbol{u}_{\mathrm{b}}$.

Then, the convergence of the familly $(\boldsymbol{T}_\varepsilon)_{\varepsilon>0}$ to $\boldsymbol{T}^+$ as $\varepsilon \longrightarrow 0$ can be expressed by the following estimate

$$\left|\left|\boldsymbol{T}_\varepsilon - \boldsymbol{T}^+\right|\right|_H \;\leq\; \left|\left|\boldsymbol{T}_{\varepsilon,\mathrm{exact}} - \boldsymbol{T}^+\right|\right|_H + ||\boldsymbol{T}_\varepsilon - \boldsymbol{T}_{\varepsilon,\mathrm{exact}}||_H$$

The first term is related to the convergence of the regularization in presence of exact data and the second term is a stability estimate which measures the propagation of the data noise. The analysis presented in [12,16] leads to a stabilty estimate of the form $||\boldsymbol{T}_\varepsilon - \boldsymbol{T}_{\varepsilon,\mathrm{exact}}||_H \leq \delta/\sqrt{\varepsilon}$ and to a convergence estimate $\left|\left|\boldsymbol{T}_{\varepsilon,\mathrm{exact}} - \boldsymbol{T}^+\right|\right|_H =$

$O(\varepsilon^\mu)$ with a constant $\mu \in]0,1]$ depending on the particular form of the operator A. Thus, we have the following convergence estimate

$$\left|\left|\boldsymbol{T}_\varepsilon - \boldsymbol{T}^+\right|\right|_H \;\leq\; C\,\varepsilon^\mu \;+\; \frac{\delta}{\sqrt{\varepsilon}} \qquad \text{with} \quad \mu \in]0,1] \;\text{ and }\; C>0 \tag{19}$$

In the ideal but highly unlikely case when the bead displacements are known exactly, the estimation (19) establishes the convergence of the $\boldsymbol{T}_\varepsilon$ to the best-approximate solution $\boldsymbol{T}^+$. In the more realistic case when the bead displacements are known only up to an error of $\delta > 0$ in the sense of (18), the estimate (19) shows that :

(i) the field $\boldsymbol{T}_\varepsilon$ calculated using the Tikhonov method explodes as $\varepsilon \longrightarrow 0$;
(ii) $\left|\left|\boldsymbol{T}_\varepsilon - \boldsymbol{T}^+\right|\right|_H$ cannot converge to zero ;
(iii) the miminal value of the error norm $\left|\left|\boldsymbol{T}_\varepsilon - \boldsymbol{T}^+\right|\right|_H$ is achievable only if the regularization parameter ε is chosen as a function of the noise level δ in order to minimize the right hand side of the estimate (19) ;
(iv) under this last optimal choice $\varepsilon(\delta)$, $\boldsymbol{T}_{\varepsilon(\delta)}$ converges to the best-approximate solution $\boldsymbol{T}^+$ as the noise level δ tends to zero.

The statement (i) is illustrated by the curves shown in Fig. 3. We have chosen the value of the regularization parameter defined in the statement (iii) using an exploration of the L–curve as described in section 5.

3. Adjoint method

Basically, applying the adjoint method to the TFM problem consists in solving a specific form of the equations (17) involved in the problem 2.5. A specific form is achieved by choosing a particular operator A involved in the *direct problem* (5). This operator expresses the weak form of a boundary value problem describing the interactions between a cell and the gel during cell migration. In this section, we start to reduce the direct problem to a 2D boundary value problem defined on the gel surface Ω. Next, we apply the theory described in section 2 in order to recover the original adjoint method applied to the TFM problem [2] and its variant obtained by taking into account the biomechanical constraints of zero resultant force [20].

In order to compare numerically the adjoint method with the FTTC method, we restrict the biomechanical constraints taken into account to the localization constraint ($\text{supp}\,(\boldsymbol{T}) \subset \overline{\Omega_c}$) and the zero resultant force ($\int_{\Omega_c} \boldsymbol{T}\,\mathrm{d}\boldsymbol{x} = 0$). Indeed, to the best of our knowledge, the FTTC method does not allow to impose the zero moment constraint ($\int_{\Omega_c} \boldsymbol{x} \wedge \boldsymbol{T}\,\mathrm{d}\boldsymbol{x} = 0$).

3.1. **Reduction to a 2D problem**

Geometry and active layer. The gel domain is modeled by the parallelepiped $\Omega_g = \Omega \times]-h_g, 0[$ in the Euclidian space $\mathbb{R}^3$ with cartesian coordinates $(x_1, x_2, x_3) = (\boldsymbol{x}, x_3)$. $\Omega \subset \mathbb{R}^2$ is the gel surface, that is the part of the boundary $\partial\Omega_g$ on which the cell migrates, and h_g is the gel thickness in the x_3 direction. The horizontal extension of Ω_g is about 2 mm while its vertical one is about 70 µm. So, from a mechanical point of view, Ω_g can be considered as a thin plate. In addition, we assume that (i) the body (gravity) and inertial forces are negligible in the whole Ω_g in comparison with the forces exerted by the cell, (ii) the vertical displacement d_3 is negligible in comparison with the horizontal ones d_1 and d_2 and (iii) the cell exerts only tangential stresses on the gel surface Ω. Under these assumptions and using dimensional analysis, Ambrosi shows [2], first that there exists an *active layer* beyond which the horizontal displacements d_1 and d_2 vanish, and, second, that in the whole Ω_g the σ_{33} component of the stress tensor can be neglected in comparison with the shear stresses exerted by the cell on the surface Ω. In mathematical terms, we have

$$x_3 \leq -h_a \quad \Longrightarrow \quad u_\alpha(\boldsymbol{x}, x_3) \approx 0 \;\; \forall (\boldsymbol{x}, x_3) \in \Omega_g \;\text{ for } \alpha = 1,2 \quad \text{and} \quad \sigma_{33} \approx 0 \;\text{ in }\; \Omega_g$$

where h_a denotes the thickness of this active layer. All these geometrical concepts are sketched in figure 2.

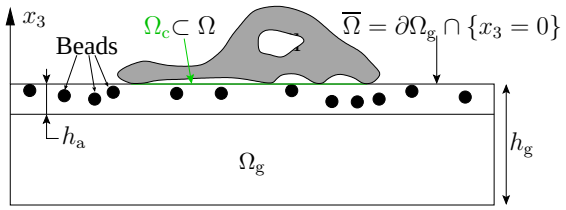

FIGURE 2. Schematic representation of a cell on the elastic substrate. Ω_g : 3D elastic subtrate ; Ω : 2D calculation domain corresponding to the cell migration plane (Ω is the interior of $\partial\Omega_\mathrm{g} \cap \{x_3 = 0\}$) ; Ω_c : cell domain, the part of Ω "below" the cell. See also the Fig. 1 page 2.

As a consequence, the first hypothesis leads to vanishing of the components σ_{13} and σ_{23} below the active layer, that is

$$\sigma_{\alpha 3} \approx 0 \quad \text{in} \quad \Omega \times]-h_\mathrm{g}, -h_\mathrm{a}[\quad \text{for } \alpha = 1, 2$$

and the second one allows us to use the plane stress approximation.

From these observations, it is possible to reduce the TFM problem to a 2D problem by using a vertical average of fields and equations across the active layer.

Depth-averaged model. The *depth–averaged operator* is (formally) defined as the map which associates to the function $\varphi : (\boldsymbol{x}, x_3) \in \Omega_\mathrm{g} \longmapsto \varphi(\boldsymbol{x}, x_3) \in \mathbb{R}$ the function $\overline{\varphi} : \boldsymbol{x} \in \Omega \longmapsto \overline{\varphi}(\boldsymbol{x}) \in \mathbb{R}$ such that $\overline{\varphi}(\boldsymbol{x}) = \frac{1}{h_\mathrm{a}} \int_{-h_\mathrm{a}}^{0} \varphi(\boldsymbol{x}, x_3) \mathrm{d}x_3$. By applying this operator to the 3D stress equilibrium equations related to directions x_1 and x_2, and by combining with the plane stress approximation of the 3D Hooke's law for isotropic and homogeneous material, we can express the relationship between the depth–averaged displacements $u_\alpha = \overline{d_\alpha}$ and the cell traction stress $\boldsymbol{T}$ as

$$\begin{aligned}
&\mathbf{div}\,\overline{\boldsymbol{\sigma}}(\boldsymbol{u}) + \boldsymbol{T} = 0 && \text{in } \Omega && (20a)\\
&\overline{\boldsymbol{\sigma}}(\boldsymbol{u}) = 2\,\mu_{2\mathrm{d}}\,\boldsymbol{\varepsilon}(\boldsymbol{u}) + \lambda_{2\mathrm{d}}\,\mathrm{div}\,\boldsymbol{u}\,\boldsymbol{I} && \text{in } \Omega && (20b)\\
&\boldsymbol{\varepsilon}(\boldsymbol{u}) = \frac{1}{2}\left(\boldsymbol{\nabla}\,\boldsymbol{u} + \boldsymbol{\nabla}\,\boldsymbol{u}^{\mathsf{T}}\right) && \text{in } \Omega && (20c)\\
&\boldsymbol{u} = 0 && \text{on } \partial\Omega && (20d)
\end{aligned}$$

where $\lambda_{2\mathrm{d}}$ and $\mu_{2\mathrm{d}}$ are the 2D Lamé's coefficients defined by

$$\mu_{2\mathrm{d}} = h_\mathrm{a}\,\frac{E}{2(1+\nu)} \quad \text{and} \quad \lambda_{2\mathrm{d}} = h_\mathrm{a}\,\frac{\nu\,E}{1-\nu^2}$$

with E and ν denote respectively the Young modulus and Poisson ratio of the substrate.

The equations (20b) and (20c) express the 2D constitutive law obtained by combining depth-averaging with the plane stress requirement. They give the depth–averaged Cauchy stress tensor $\overline{\boldsymbol{\sigma}}(\boldsymbol{u})$ as a function of the the linearized strain tensor $\boldsymbol{\varepsilon}(\boldsymbol{u})$ related to depth–averaged displacements. The boundary condition (20d) results from the 3D boundary conditions which impose zero displacements on the lateral part of the boundary $\partial\Omega_\mathrm{g}$.

Data needed to the adjoint method. The Tikhonov functional J_ε defined by (6) compares $A^{-1}\boldsymbol{T}$ with the experimental data $\boldsymbol{u}_\mathrm{b}$. So, since $A^{-1}\boldsymbol{T}$ must be the solution of the direct problem (20), that is $A^{-1}\boldsymbol{T}$ must be a depth–averaged displacement, strictly speaking we need the experimental data $\boldsymbol{u}_\mathrm{b}$ to involve depth–averaged values. This is true if the beads are uniformely dispersed along the vertical direction in the gel.

3.2. **Direct problem**

Functional spaces. The spaces H for traction stresses and V for gel displacements are chosen in order to define the solution of the boundary value problem (20) in the weak sense. Thus we use usual Lebesgue and Sobolev spaces

$$H = \boldsymbol{L}^2(\Omega) = L^2(\Omega) \times L^2(\Omega) \quad \text{and} \quad V = \boldsymbol{H}^1_0(\Omega) = H^1_0(\Omega) \times H^1_0(\Omega)$$

equipped with their usual scalar products [1, 7], that is $(\boldsymbol{u},\boldsymbol{v})_H = (\boldsymbol{u},\boldsymbol{v})_{\boldsymbol{L}^2(\Omega)} = \int_\Omega \boldsymbol{u}\cdot\boldsymbol{v}\,\mathrm{d}\boldsymbol{x}$ and $(\boldsymbol{u},\boldsymbol{v})_V = (\boldsymbol{u},\boldsymbol{v})_{\boldsymbol{H}^1_0(\Omega)} = \int_\Omega \boldsymbol{\nabla}\,\boldsymbol{u} : \boldsymbol{\nabla}\,\boldsymbol{v}\,\mathrm{d}\boldsymbol{x}$ where $\boldsymbol{\nabla}\,\boldsymbol{u} : \boldsymbol{\nabla}\,\boldsymbol{v} = \Sigma_{i,j}\partial_j u_i\,\partial_j v_i$. Therefore, we have $V' = \boldsymbol{H}^{-1}(\Omega) = H^{-1}(\Omega)\times H^{-1}(\Omega)$ and the Gelfand triple property (2) holds [1, 7].

Direct problem. The elasticity operator A results from the weak form of the boundary value problem (20). Therefore, if we define the bilinear $a(\cdot,\cdot)$ on $\boldsymbol{H}^1_0(\Omega)\times\boldsymbol{H}^1_0(\Omega)$ by

$$a(\boldsymbol{u},\boldsymbol{v}) \;=\; 2\,\mu_{2\mathrm{d}}\int_\Omega \boldsymbol{\varepsilon}\,(\boldsymbol{u}) : \boldsymbol{\varepsilon}\,(\boldsymbol{v})\;\mathrm{d}\boldsymbol{x} \;+\; \lambda_{2\mathrm{d}}\int_\Omega \operatorname{div}\boldsymbol{u}\,\operatorname{div}\boldsymbol{v}\,\mathrm{d}\boldsymbol{x} \quad \forall\,\boldsymbol{u},\boldsymbol{v}\in\boldsymbol{H}^1_0(\Omega) \tag{21a}$$

we choose the operator A as the element of $\mathscr{L}\left(\boldsymbol{H}^1_0(\Omega),\boldsymbol{H}^{-1}(\Omega)\right)$ defined by

$$\langle A\,\boldsymbol{u},\boldsymbol{v}\rangle_{V',V} \;=\; a(\boldsymbol{u},\boldsymbol{v}) \quad \forall\,\boldsymbol{u},\boldsymbol{v}\in\boldsymbol{H}^1_0(\Omega) \tag{21b}$$

The direct problem related to this operator is well-posed as it is showed in the following proposition.

Proposition 3.1. *The elasticity operator defined by* (21) *satisfies the* $\boldsymbol{H}^1_0(\Omega)$*–ellipticity condition* (4) *and defines a self-adjoint isomorphism from* $\boldsymbol{H}^1_0(\Omega)$ *to* $\boldsymbol{H}^{-1}(\Omega)$ *:* $A\in$ *Isom* $\left(\boldsymbol{H}^1_0(\Omega),\boldsymbol{H}^{-1}(\Omega)\right)$ *and* $A^{\mathsf{T}} = A$*.*

Démonstration. The $\boldsymbol{H}^1_0(\Omega)$–ellipticity results from the classical Korn inequality [9] and then the isomorphism property results from the Lax-Milgram lemma [7]. The self-adjonction of A is a direct consequence of the definition (21). □

3.3. **Observation operator**

Data space and observation operator. We assume that the data is continuous in the sense that experimental beads displacements $\boldsymbol{u}_{\mathrm{b}}$ are known in a subset $\Omega_{\mathrm{b}}\subsetneq\Omega$ which has a non zero Lebesgue measure ($|\Omega_{\mathrm{b}}|>0$). The case of pointwise data is considered in [25]. So the data $\boldsymbol{u}_{\mathrm{b}}$ must be at least a function defined on Ω_{b}. But, as indicated in section 2, the space X_{b} must be a Hilbert space which can be identified with its dual without contravening to the identification $\boldsymbol{L}^2(\Omega)'\equiv\boldsymbol{L}^2(\Omega)$. To meet these requirements, we define the Hilbert space X_{b} as the following closed subspace of $\boldsymbol{L}^2(\Omega)$

$$X_{\mathrm{b}} \;=\; \left\{\,\boldsymbol{v}\in\boldsymbol{L}^2(\Omega)\;;\;\operatorname{supp}(\boldsymbol{v})\subset\overline{\Omega_{\mathrm{b}}}\,\right\} \tag{22}$$

and the value taken by the observation operator B when evaluated at $\boldsymbol{v}\in\boldsymbol{H}^1_0(\Omega)$ as

$$B\,\boldsymbol{v}\;:\;\boldsymbol{x}\in\Omega\longmapsto(B\,\boldsymbol{v})\,(\boldsymbol{x}) = \chi_{\mathrm{b}}(\boldsymbol{x})\,\boldsymbol{v}(\boldsymbol{x})\in\mathbb{R}^2 \tag{23}$$

where $\chi_{\mathrm{b}}(\cdot)$ stands for the characteristic function of the subset Ω_{b} ($\chi_{\mathrm{b}}(\boldsymbol{x})=1$ if $\boldsymbol{x}\in\Omega_{\mathrm{b}}$ and $\chi_{\mathrm{b}}(\boldsymbol{x})=0$ if $\boldsymbol{x}\in\Omega\setminus\Omega_{\mathrm{b}}$). Thanks to the Poincaré inequality [1, 7], it is clear that $B\in\mathscr{L}\left(\boldsymbol{H}^1_0(\Omega),X_{\mathrm{b}}\right)$. But, there exists another way to interpret the operator B, a way that will allow to simplify the application of equations (17).

Proposition 3.2 (**Structure of the observation operator**). *Let* P_{b} *be the* $\boldsymbol{L}^2(\Omega)$*–orthogonal projection operator from* $\boldsymbol{L}^2(\Omega)$ *onto* X_{b}*. Then, the observation operator* $B\in\mathscr{L}\left(\boldsymbol{H}^1_0(\Omega),X_{\mathrm{b}}\right)$ *defined by* (23) *satisfies*

(1) *B is the restriction to $\boldsymbol{H}^1_0(\Omega)$ of P_b, that is $B = P_\mathrm{b}{}_{|\boldsymbol{H}^1_0(\Omega)}$;*
(2) *B is self–adjoint ($B^\mathsf{T} = B$) and idempotent ($BB = B$).*

Démonstration. As X_b is a closed subspace of $\boldsymbol{L}^2(\Omega)$, the value of P_b evaluated at $\boldsymbol{v} \in \boldsymbol{L}^2(\Omega)$ is characterized by [7, 10] $P_\mathrm{b}\,\boldsymbol{v} \in X_\mathrm{b}$ and $(\boldsymbol{v} - P_\mathrm{b}\,\boldsymbol{v}, \boldsymbol{\varphi})_{\boldsymbol{L}^2(\Omega)} = 0\ \forall \boldsymbol{\varphi} \in X_\mathrm{b}$. Hence, it is easy to verify that $P_\mathrm{b}\,\boldsymbol{v}$ is defined as the function $P_\mathrm{b}\,\boldsymbol{v} \,:\, \boldsymbol{x} \in \Omega \longmapsto (P_\mathrm{b}\boldsymbol{v})(\boldsymbol{x}) = \chi_\mathrm{b}(\boldsymbol{x})\,\boldsymbol{v}(\boldsymbol{x}) \in \mathbb{R}^2$. By comparison with definition (23) the first point holds. The second point is a property of the projection onto a closed subspace. □

3.4. Constrained space and projection operator

Constrained space and projection operator. As indicated in the introduction of this section, we restrict the set of biomechanical constraints to the ones that the FTTC method can handle. Thus, we choose the constrained space H_c as

$$H_\mathrm{c} \;=\; \left\{ \boldsymbol{T} \in \boldsymbol{L}^2(\Omega)\ ;\ \mathrm{supp}\,(\boldsymbol{T}) \subset \overline{\Omega_\mathrm{c}} \quad \text{and} \quad \int_{\Omega_\mathrm{c}} \boldsymbol{T}\,\mathrm{d}\boldsymbol{x} = 0 \right\} \tag{24}$$

It is clear that H_c is a closed subspace of $\boldsymbol{L}^2(\Omega)$.

To use the abstract equations (17), it remains to identify the projection operator P_c.

Proposition 3.3 (**Structure of the projection operator**). *The projection operator P_c belongs to the space $\mathscr{L}\left(\boldsymbol{L}^2(\Omega), \boldsymbol{L}^2(\Omega)\right)$ and for all $\boldsymbol{T} \in \boldsymbol{L}^2(\Omega)$, the element $P_\mathrm{c}\,\boldsymbol{T}$ is characterized by*

$$P_\mathrm{c}\,\boldsymbol{T} \,:\, \boldsymbol{x} \in \Omega \longmapsto (P_\mathrm{c}\,\boldsymbol{T})\,(\boldsymbol{x}) = \chi_\mathrm{c}(\boldsymbol{x})\ (\boldsymbol{T}(\boldsymbol{x}) - \boldsymbol{T}_{\Omega_\mathrm{c}}) \ \in \mathbb{R}^2 \tag{25a}$$

where $\boldsymbol{T}_{\Omega_\mathrm{c}}$ and $\chi_\mathrm{c}(\cdot)$ denote respectively the average value of $\boldsymbol{T}$ over Ω_c and the characteristic function of Ω_c

$$\boldsymbol{T}_{\Omega_\mathrm{c}} = \frac{1}{|\Omega_\mathrm{c}|}\int_{\Omega_\mathrm{c}} \boldsymbol{T}\,\mathrm{d}\boldsymbol{x} \qquad \textit{and} \qquad \chi_\mathrm{c}(\boldsymbol{x}) = \left\{ \begin{array}{ll} 1 & \textit{if}\ \ \boldsymbol{x} \in \Omega_\mathrm{c} \\ 0 & \textit{if}\ \ \boldsymbol{x} \in \Omega \setminus \Omega_\mathrm{c} \end{array} \right. \tag{25b}$$

Démonstration. The proof is very similar to proof of proposition 3.2. First, the function $P_\mathrm{c}\boldsymbol{T}$ defined by (25a) belongs to the space H_c defined in (24). Next, for all $\boldsymbol{\varphi} \in \boldsymbol{L}^2(\Omega)$ we have $(\boldsymbol{T} - P_\mathrm{c}\boldsymbol{T}, \boldsymbol{\varphi})_{\boldsymbol{L}^2(\Omega)} = (\boldsymbol{T}_{\Omega_\mathrm{c}}, \boldsymbol{\varphi})_{\boldsymbol{L}^2(\Omega_\mathrm{c})} = |\Omega_\mathrm{c}|\boldsymbol{T}_{\Omega_\mathrm{c}}\boldsymbol{\varphi}_{\Omega_\mathrm{c}}$. So, if we choose $\boldsymbol{\varphi}$ in the space H_c, we can write that $(\boldsymbol{T} - P_\mathrm{c}\boldsymbol{T}, \boldsymbol{\varphi})_{\boldsymbol{L}^2(\Omega)} = 0\ \forall \boldsymbol{\varphi} \in H_\mathrm{c}$. Hence, the function $P_\mathrm{c}\boldsymbol{T}$ defined by (25a) is the $\boldsymbol{L}^2(\Omega)$–orthogonal projection of $\boldsymbol{T} \in \boldsymbol{L}^2(\Omega)$ onto the constrained space H_c. □

3.5. Solving the TFM problem by using adjoint method

By combining the results of the current section with the theory developed in section 2, we can develop the direct formulation of the TFM problem 2.5 with the constrained space H_c and the data space X_b respectively defined by (24) and (22).

Problème 3.4. (**Direct formulation of the TFM**) Given $\boldsymbol{u}_\mathrm{b} \in X_\mathrm{b}$ and $\varepsilon > 0$, find $(\boldsymbol{p}_\varepsilon, \boldsymbol{u}_\varepsilon) \in \boldsymbol{H}^1_0(\Omega) \times \boldsymbol{H}^1_0(\Omega)$ solution of the following variational equations

$$a(\boldsymbol{p}_\varepsilon, \boldsymbol{q}) \;-\; \int_\Omega \chi_\mathrm{b}\,\boldsymbol{u}_\varepsilon \cdot \boldsymbol{q}\,\mathrm{d}\boldsymbol{x} \;=\; -\int_\Omega \chi_\mathrm{b}\,\boldsymbol{u}_\mathrm{b} \cdot \boldsymbol{q}\,\mathrm{d}\boldsymbol{x} \qquad \forall\, \boldsymbol{q} \in \boldsymbol{H}^1_0(\Omega) \tag{26a}$$

$$\frac{1}{\varepsilon}\int_\Omega \chi_\mathrm{c}\,\boldsymbol{p}_\varepsilon \cdot \boldsymbol{v}\,\mathrm{d}\boldsymbol{x} \;-\; \frac{1}{\varepsilon}\frac{1}{|\Omega_\mathrm{c}|}\int_{\Omega_\mathrm{c}} \boldsymbol{p}_\varepsilon\,\mathrm{d}\boldsymbol{x}\int_\Omega \boldsymbol{v}\,\mathrm{d}\boldsymbol{x} \;+\; a(\boldsymbol{u}_\varepsilon, \boldsymbol{v}) \;=\; 0 \qquad \forall\, \boldsymbol{v} \in \boldsymbol{H}^1_0(\Omega) \tag{26b}$$

where the bilinear form $a(\cdot,\cdot)$ is defined in (21). Then, deduce $\boldsymbol{T}_\varepsilon \in H_\mathrm{c}$ by

$$\boldsymbol{T}_\varepsilon = -\frac{1}{\varepsilon}\left(\chi_\mathrm{c}\,\boldsymbol{p}_\varepsilon \;-\; \frac{1}{|\Omega_\mathrm{c}|}\int_{\Omega_\mathrm{c}} \boldsymbol{p}_\varepsilon \,\mathrm{d}\boldsymbol{x}\right) \tag{27}$$

The two weak equations (26) can be interpreted in the usual way as the following two coupled Lamé-Navier-like partial diffential equations

$$\begin{array}{rcll} -\mu_\mathrm{2d}\,\Delta\boldsymbol{p}_\varepsilon \;-\; (\lambda_\mathrm{2d}+\mu_\mathrm{2d})\,\boldsymbol{\nabla}\,\mathrm{div}\,\boldsymbol{p}_\varepsilon & = & \chi_\mathrm{b}\,\boldsymbol{u}_\varepsilon - \boldsymbol{u}_\mathrm{b} & \text{in } \Omega \\ -\mu_\mathrm{2d}\,\Delta\boldsymbol{u}_\varepsilon \;-\; (\lambda_\mathrm{2d}+\mu_\mathrm{2d})\,\boldsymbol{\nabla}\,\mathrm{div}\,\boldsymbol{u}_\varepsilon & = & \dfrac{1}{\varepsilon}\,\chi_\mathrm{c}\,\boldsymbol{p}_\varepsilon \;-\; \dfrac{1}{\varepsilon}\,\dfrac{1}{|\Omega_\mathrm{c}|}\displaystyle\int_{\Omega_\mathrm{c}} \boldsymbol{p}_\varepsilon \,\mathrm{d}\boldsymbol{x} & \text{in } \Omega \end{array}$$

under the homogeneous Dirichlet boundary conditions

$$\boldsymbol{u}_\varepsilon \;=\; 0 \quad \text{and} \quad \boldsymbol{p}_\varepsilon \;=\; 0 \quad \text{on} \quad \partial\Omega$$

Numerical method. The weak equations (26) are discretized by a finite element method using local linear interpolation (P_1 element) on an unstructured mesh. The geometrical flexibility of the meshing tools allows to assign all the bead locations as nodes in the computational mesh and to handle the cell domain Ω_c as a specific subdomain in the mesh. In particular, the cell filipodia can be taken into account in the mesh. The linear system of discretized equations is numerically solved by using the bi-conjugate gradient method with diagonal preconditioning.

4. FTTC method

Mathematically, the FTTC method is of the same nature as the adjoint method. It also consists in solving the problem 2.5 in which the operator A takes a specific form. This form is described in section 4.1. The particularity of the FTTC method is that the resolution of the direct problem related to this operator is achieved by use of the Fourier analysis. Section 4.2 summarizes the results of the Fourier analysis used by the FTTC method. Section 4.3 presents the classical FTTC method as well as its conditions and limits of applicability. In section 4.4, we conclude by introducing an improved version of the FTTC method satisfying to the localization constraint.

4.1. **Reduction to a 2D problem**

Under the assumptions that the gel material presents a linear, homogeneous and isotropic behavior, and that the external forces reduce to the forces imposed by the cell, the 3D displacement field $\boldsymbol{d} : (\boldsymbol{x}, x_3) \in \Omega_\mathrm{g} \longmapsto \boldsymbol{d}(\boldsymbol{x}, x_3) \in \mathbb{R}^3$ can be expressed as a linear function depending on the traction stress field $\boldsymbol{T} : \boldsymbol{x} \in \Omega_\mathrm{c} \longmapsto \boldsymbol{T}(\boldsymbol{x}) \in \mathbb{R}^2$ exerted by the cell on the gel surface. At least formally, this linear function takes the form of an integral representation which is nothing but the convolution product $\mathbb{G} * \boldsymbol{T}_\mathrm{3d}$ between the Green Tensor $\mathbb{G}_\mathrm{3d}$ of the Boussinesq-Cerruti problem [17] and $\boldsymbol{T}_\mathrm{3d} = [T_1, T_2, 0] = [\boldsymbol{T}, 0]$:

$$\boldsymbol{d}(\boldsymbol{x}, x_3) = \int_{\boldsymbol{x}' \in \Omega_\mathrm{c}} \mathbb{G}_\mathrm{3d}\,(\boldsymbol{x} - \boldsymbol{x}', x_3 - x_3')\;\boldsymbol{T}_\mathrm{3d}(\boldsymbol{x}', x_3')\,\mathrm{d}s(\boldsymbol{x}') \qquad \forall (\boldsymbol{x}, x_3) \in \Omega_\mathrm{g}$$

Hence, the reduction to a 2D problem defined on the migrating plane Ω of the cell is achieved by evaluating the previous relation on Ω, that is for $\boldsymbol{x} \in \Omega$ and $x_3 = 0$, and using only the components associated with directions x_1 and x_2. So, the integral form of the abstract operator A^{-1} can be written in the following form :

$$\boldsymbol{u} = A^{-1}\boldsymbol{T} \quad \Longleftrightarrow \quad \boldsymbol{u}(\boldsymbol{x}) = (\mathbb{G} * \boldsymbol{T})(\boldsymbol{x}) = \int_{\boldsymbol{x}' \in \Omega_c} \mathbb{G}(\boldsymbol{x} - \boldsymbol{x}')\ \boldsymbol{T}(\boldsymbol{x}')\, \mathrm{d}s(\boldsymbol{x}') \qquad \forall \boldsymbol{x} \in \Omega \tag{28}$$

When Ω_g is the half-space $\mathbb{R}^2 \times \mathbb{R}^{-\star}$, the expression of the Green tensor $\mathbb{G}_{3d}$ is rigorously established in [17] and leads to the 2D reduction :

$$\mathbb{G}(\boldsymbol{x}) = \frac{1+\nu}{\pi\, E}\, \frac{1}{|\boldsymbol{x}|^3} \begin{pmatrix} (1-\nu)|\boldsymbol{x}|^2 + \nu\, x_1^2 & \nu\, x_1\, x_2 \\ \nu\, x_1\, x_2 & (1-\nu)|\boldsymbol{x}|^2 + \nu\, x_2^2 \end{pmatrix} \quad \text{for all } \ \boldsymbol{x} \in \Omega \quad \textit{or} \quad \in \mathbb{R}^2 \tag{29}$$

where $|\boldsymbol{x}| = \sqrt{x_1^2 + x_2^2}$.

Remarque 4.1. The geometrical assumptions used by the adjoint and the FTTC methods are very different. The first one assumes that the gel domain can be approximated by a thin plate while the second one assumes that it is thick enough to be considered as a half-space.

The equations (28) and (29) form the basis of the BEM [11] and the FTTC method [8].

4.2. **Fourier analysis for the TFM problem**

In this section we recall some classical results of Fourier analysis used here. All these results are established in [27] for the 1D case. These results are presented for a generic function denoted by f which should be interpreted as a component of the vectors $\boldsymbol{T}$ or $\boldsymbol{u}$ or the tensor $\mathbb{G}$.

Continuous Fourier transform. We denote by $\widehat{f}$, or equivalently $\mathcal{F}f$, the 2D Fourier transform of the scalar complex–valued function $f : \boldsymbol{x} \in \mathbb{R}^2 \longmapsto f(\boldsymbol{x}) \in \mathbb{C}$. The Fourier transform $\widehat{f} = \mathcal{F}f$ of the function f is defined by

$$\widehat{f}(\boldsymbol{\xi}) \ = \langle \mathcal{F}f, \boldsymbol{\xi} \rangle \ = \ \int_{\mathbb{R}^2} f(\boldsymbol{x})\, \exp(-i 2\pi\, \boldsymbol{x} \cdot \boldsymbol{\xi})\, \mathrm{d}\boldsymbol{x} \quad \forall\, \boldsymbol{\xi} \in \mathbb{R}^2 \tag{30}$$

where $\boldsymbol{\xi}$ denotes the wave vector (the generic element of the Fourier space) and $i = \sqrt{-1}$.

The Fourier transform $\widehat{f}$ is clearly well-defined when $f \in L^1(\mathbb{R}^2)$. By using the density of the rapidly decreasing functions space $\mathscr{S}(\mathbb{R}^2)$ (the Schwartz space) into $L^2(\mathbb{R}^2)$, the operator $\mathcal{F}$ can be extended to $L^2(\mathbb{R}^2)$ to define an isomorphism from $\boldsymbol{L}^2(\mathbb{R}^2)$ into $\boldsymbol{L}^2(\mathbb{R}^2)$.

The components of the traction stress $\boldsymbol{T}$ and the displacement $\boldsymbol{u}$ belong to $L^2(\Omega)$. So, in order to use the Fourier analysis, these fields are extended to be zero on $\mathbb{R}^2 \setminus \Omega$ to define functions belonging to $L^2(\mathbb{R}^2)$.

Continuous Fourier transform and convolution. When f and g are two functions belonging to $L^2(\mathbb{R}^2)$ their convolution product $f * g$ is an element of the tempered distributions space $\mathscr{S}'(\mathbb{R}^2)$. So, the Fourier transform $\widehat{f * g}$ exists and satisfies the well-know identity

$$\widehat{f * g} = \widehat{f}\,\widehat{g} \qquad \text{in } \mathscr{S}'(\mathbb{R}^2) \tag{31}$$

This last identity is the basis of the FTTC method.

Discrete Fourier transform and sampling. Usually the numerical approximation of the Fourier coefficients (30) is performed by using specialized and optimized algorithms [13]. These algorithms are implementations of the so-called *discrete Fourier transform* (DFT). In the TFM context, the DFT approximates the integrals (30) by using the rectangle method (left-bottom endpoint rule) on a uniform and structured grid whose nodes are the points $\boldsymbol{x}_{\boldsymbol{n}} = (n_1\, h_1, n_2\, h_2)$, where h_k and n_k are respectively the spatial steps and the index in the direction x_k of the physical space, with $\boldsymbol{n} = (n_1, n_2)$. When practical computations are performed, the steps sizes and

the number of nodes N_k in the x_k–direction are chosen so that all nodes belong to Ω for $n_k = 0, 1, \cdots, N_k - 1$. But, for theoretical convenience, we can consider that this grid covers the whole $\mathbb{R}^2$ in the same manner that the functions are extended by zero on $\mathbb{R}^2 \setminus \Omega$.

As a matter of fact, the DFT is more than a way to approximate the integrals (30). Mathematically, the DFT approximates the Fourier transform of the tempered distribution $f_{\mathrm{s}} = \sum_{\boldsymbol{n}\in\mathbb{Z}^2} f(\boldsymbol{x_n})\, \delta_{\boldsymbol{x_n}}$ where $\delta_{\boldsymbol{x_n}}$ is the Dirac measure concentrated at node $\boldsymbol{x_n}$. This distribution is called the *sampling* of f related to the nodes $\boldsymbol{x_n}$. The Fourier transform of the sampling f_{s} is the tempered distribution that, for sake of simplicity, we write as the function :

$$\widehat{f}_{\mathrm{s}}(\boldsymbol{\xi}) = \frac{1}{h_1\, h_2} \sum_{\boldsymbol{n}\in\mathbb{Z}^2} \widehat{f_{\boldsymbol{n}}}\,(\boldsymbol{\xi}) \quad \text{with} \quad \widehat{f_{\boldsymbol{n}}}\,(\boldsymbol{\xi}) = \widehat{f}\,(\xi_1 - n_1/h_1, \xi_2 - n_2/h_2) \quad \forall\, \boldsymbol{\xi} = (\xi_1, \xi_2) \in \mathbb{R}^2 \tag{32}$$

The distributions $\widehat{f_{\boldsymbol{n}}}$ are the *translated spectra*. The distribution $\widehat{f}_{\mathrm{s}}$ is periodic with period $\boldsymbol{p} = (1/h_1, 1/h_2)$. So, by using the $N_1\, N_2$ values of the function f at the spatial nodes $\boldsymbol{x_n}$, the DFT can approximate $\widehat{f}_{\mathrm{s}}$ at $N_1\, N_2$ nodes defined in the Fourier Space and contained in one period of $\widehat{f}_{\mathrm{s}}$; for example at the nodes

$$\boldsymbol{\xi_n} = \left(\frac{2n_1 - N_1}{2N_1 h_1}, \frac{2n_2 - N_2}{2N_2 h_2} \right) \quad \text{for } n_k = 0, 1, \cdots, N_k - 1 \tag{33}$$

It is natural to think that this approximation of $\widehat{f}_{\mathrm{s}}$ yields also an approximation of the continuous Fourier transform $\widehat{f}$. This is true if certain extra conditions are met.

Approximation of the continuous Fourier transform. If the function f and the spatial grid satisfy the following conditions

$$\exists\, \lambda_{\mathrm{c},1},\, \lambda_{\mathrm{c},2} \in \mathbb{R} \;\text{ such that } |\xi_k| \geq \lambda_{\mathrm{c},k} \implies \widehat{f}(\boldsymbol{\xi}) = 0 \tag{34a}$$

$$\lambda_{\mathrm{c},k} \leq \frac{1}{2\, h_k} \tag{34b}$$

the approximation of the Fourier coefficients $\widehat{f}_{\mathrm{s}}\,(\boldsymbol{\xi_n})$ obtained using the DFT is also an approximation of the Fourier transform $\widehat{f}$ evaluated at node $\boldsymbol{\xi_n}$ in Fourier space.

Indeed, the condition (34a) means that the support of the (tempered) distribution $\widehat{f}$ is included in $[-\lambda_{\mathrm{c},1}, \lambda_{\mathrm{c},1}] \times [-\lambda_{\mathrm{c},2}, \lambda_{\mathrm{c},2}]$. Therefore, thanks to the Nyquist condition (34b), the supports of two translated distributions $\widehat{f_{\boldsymbol{n}}}$ defined in (32) do not intersect if these distributions correspond to two distinct values of the multi-index $\boldsymbol{n}$. As a consequence, no overlapping occurs during the summation (32) of the $\widehat{f_{\boldsymbol{n}}}$ and then, over each interval of the form $[-h_1/2 + k_1 N_1, h_1/2 + k_1 N_1[\times [-h_2/2 + k_2 N_2, h_2/2 + k_2 N_2[$ for $k_1, k_2 \in \mathbb{Z}$, the Fourier transforms $\widehat{f}$ and $\widehat{f}_{\mathrm{s}}$ coincide.

In practice, the condition (34a) is only approximatively satisfied. However, it can be enforced by using a filtering technique. By contrast, the Nyquist condition is satisfied if the steps sizes of the spatial grid are chosen sufficiently small.

Since the DFT approximates the integrals involved in the Fourier coefficients (30) by using the rectangle method, the accuracy of the FTTC method is equivalent to the accuracy of a P_0 finite element method.

4.3. **The classical FTTC method**

The FTTC method as an alternative to the BEM. The FTTC method [8] and the BEM [11] are closely related in the sense that the FTTC method can be regarded as an attempt to improve and simplify the BEM. The BEM consists in writing the equation (28) for $\boldsymbol{x}$ describing the beads locations ($\boldsymbol{x} \in \Omega_{\rm b}$, $\Omega_{\rm b}$ being here a discrete and finite set of isolated points) and with $\boldsymbol{u}(\boldsymbol{x})$ substituted by the experimental beads displacements $\boldsymbol{u}_{\rm b}$. After a discretization of the cell domain $\Omega_{\rm c}$ using a suitable unstructured mesh and by using a Tikhonov regularization method, the BEM characterizes the nodal values of the stress vector $\boldsymbol{T}$ as the solution of a large and dense system of linear equations. The reduction of computation time used by the numerical resolution of this system and the difficulty to set a suitable value for the regularization parameter were the main motivations for introducing the FTTC method.

Concerning the computational cost, the FTTC exploits the fact that the convolution product involved in the integral form (28) becomes a simple product in the Fourier space in the sense of (31). The FTTC method in its original form [8] *does not use any apparent regularization* procedure ; the necessity of such procedure was shown subsequently by Sabass *et al.* [21].

Principles of the FTTC method. The principles of the FTTC method can be summarized as follows. The computationl domain Ω is a rectangle where the spatial variable is discretized using a uniform regular grid whose nodes $\boldsymbol{x_n}$ are defined in section 4.2. Experimental bead displacements $\boldsymbol{u}_{\rm b}$ are replaced by their interpolated values $\boldsymbol{u}_{\rm g}$ on this regular grid. For each wave vector $\boldsymbol{\xi_n}$ of the induced uniform grid in Fourier space, equation (28) is inverted in the complex plane $\mathbb{C}^2$ thanks to property (31) and yields the Fourier transform of the stress vector $\widehat{\boldsymbol{T}}(\boldsymbol{\xi_n}) = \widehat{\mathbb{G}}(\boldsymbol{\xi_n})^{-1}\, \widehat{\boldsymbol{u}_{\rm b}}(\boldsymbol{\xi_n})$. The Fourier components of the traction stress are then transformed back into the physical space using the inverse Fourier transform $T_k = \mathcal{F}^{-1}\widehat{T_k}$ for $k = 1, 2$.

Application of the Fourier transform (30) to the Green tensor defined by (29) in the physical space leads to the following expression for the Green tensor in the Fourier space

$$\widehat{\mathbb{G}}(\boldsymbol{\xi}) \;=\; \frac{1+\nu}{\pi\, E}\, \frac{1}{|\boldsymbol{\xi}|^3} \begin{bmatrix} (1-\nu)\,|\boldsymbol{\xi}|^2 + \nu\xi_2^2 & -\nu\,\xi_1\xi_2 \\ -\nu\,\xi_1\xi_2 & (1-\nu)\,|\boldsymbol{\xi}|^2 + \nu\xi_1^2 \end{bmatrix} \quad \text{for all wave vectors } \boldsymbol{\xi} \in \mathbb{R}^2 \tag{35}$$

In practice, the direct and inverse Fourier transforms are performed by using the FFT implementation [13] of the direct and inverse DFT. When the FTTC method was introduced [8], it did not use any regularization procedure. But since recently [21], it is widely known that the FTTC method must be used together with a regularization scheme (see the following section for the algorithmic aspects).

Data needed for the FTTC method. As showed in the above principles, the FTTC method needs the knowledge of the experimental beads displacements at every point on the spatial grid used for the discretization of the gel surface. But in practice, experimental data are avaible only on scattered points in Ω. So, the implementation of the FTTC method need a supplementary *interpolation* operator which estimates the values $\boldsymbol{u}_{\rm g}$ of gel displacements on a regular grid from the knowledge of the experimental beads displacements $\boldsymbol{u}_{\rm b}$. This aspect of the FTTC method is rarely developped in the literature. We consider this issue in section 4.4.

What biomechanical constraints are satisfied ? Since BEM is based on the convolution integral (28), the traction stresses $\boldsymbol{T}$ necessarily satisfy the localization constraint $\mathrm{supp}\,(\boldsymbol{T}) \subset \Omega_{\rm c}$. The classical FTTC method does not allow to satisfy this constraint. Nevertheless, the original paper [8] proposes an iterative variant of the FTTC method, the so-called *constrained*–FTTC, which should satisfy this constraint. But, no convergence result of this variant has been proved. Furthermore, the constrained-FTTC modifies the experimental beads displacements.

By contrast, the FTTC method allows to impose *a* zero resultant force, however this is done over the whole computation domain. The FTTC method imposes $\int_\Omega \boldsymbol{T}\,\mathrm{d}\boldsymbol{x} = 0$ while, in general, $\int_{\Omega_{\rm c}} \boldsymbol{T}\,\mathrm{d}\boldsymbol{x} \neq 0$. Indeed [8],

the resultant force is nothing else than the Fourier coefficient corresponding to the zero wave vector, that is $\int_\Omega \boldsymbol{T}\,\mathrm{d}\boldsymbol{x} = \widehat{\boldsymbol{T}}(\boldsymbol{\xi})_{|\boldsymbol{\xi}=\mathbf{0}}$. So, the constraint $\int_\Omega \boldsymbol{T}\,\mathrm{d}\boldsymbol{x} = 0$ is imposed directly in the Fourier space by setting $\widehat{\boldsymbol{T}}(\boldsymbol{\xi})_{|\boldsymbol{\xi}=\mathbf{0}} = \mathbf{0}$.

The zero moment constraint $\int_{\Omega_\mathrm{c}} \boldsymbol{x} \wedge \boldsymbol{T}\,\mathrm{d}\boldsymbol{x} = 0$ is not addressed in the FTTC litterature. Furthermore, mathematically, this constraint cannot be imposed in the Fourier space.

The table 1 below summarizes the main characteristics of the currently used methods to solve the TFM problem.

Method	$\mathrm{supp}\,(\boldsymbol{T}) \subset \overline{\Omega_\mathrm{c}}$	$\int_{\Omega_\mathrm{c}} \boldsymbol{T}\,\mathrm{d}\boldsymbol{x} = 0$	$\int_{\Omega_\mathrm{c}} \boldsymbol{x} \wedge \boldsymbol{T}\,\mathrm{d}\boldsymbol{x} = 0$	data preservation
BEM	yes	no	no	yes
FTTC	no	yes$^{(1)}$	no	no$^{(2)}$
p–FTTC	yes	yes$^{(1)}$	no	no$^{(2)}$
AM–direct	yes	yes	no	yes
AM–dual	yes	yes	yes	yes

TABLEAU 1. Main characteristics of the current methods for solving the TFM problem. The p–FTTC method is introduced in section 4.4. AM–direct is the adjoint method presented in section 3 and defined by constrained space (24) and the equations (26) and (27). AM–dual is the adjoint method described in [25]. $^{(1)}$ The FTTC and p–FTTC methods impose only that $\int_{\mathrm{supp}(\boldsymbol{T})} \boldsymbol{T}\,\mathrm{d}\boldsymbol{x} = 0$ and $^{(2)}$ use interpolated data.

Conditions of use and limits of applicability. Two limits of applicability of the FTTC method exist. The first one concerns the validity of the formulation and the second one is related to the accuracy of the numerical DFT.

The validity of the formulation used to define the direct problem (28) is equivalent to that of the expression (29) of the Green tensor. Hence, it is equivalent to the possibility to approximate the 3D gel domain by a half-plane.

The accuracy which we are discussing here is not the accuracy of the quadrature formula used to approximate the Fourier coefficients (30) but the capacity of the DFT to avoid the overlap of the translated spectra $\widehat{f_{\boldsymbol{n}}}$ during summation (32). It only concerns the (interpolated) beads displacements since the exact Fourier transform of the Green tensor is available thanks to (35). As indicated in section 4.2, the conditions (34) are sufficient to achieve this kind of accuracy. If these conditions are not satisfied, then the computed Fourier transform of the beads displacements is a poor approximation. In the context of inverse problems, this loss of accuracy can be dramatic. To avoid these difficulties, it is sufficient to choose a spatial step size h_k small enough in order to satisfy condition (34b).

4.4. **The projected FTTC method (p–FTTC)**

Principles. The analysis of the TFM problem developed in the section 2 pointed out the role of the different "ingredients". In particular, the formulation obtained with equations (17) splits the solution method into two main parts. First, we determine the adjoint state $\boldsymbol{p}_\varepsilon$ and the corresponding optimal displacement $\boldsymbol{u}_\varepsilon$ by solving the abstract variational equations (17b) and (17a), which define an unconstrained problem when the projection operator P_c is explicitly known. Then, we deduce the optimal stress field $\boldsymbol{T}_\varepsilon$ by projecting the adjoint state onto the subspace related to the biomechanical constraints. We will use this decoupling approach to define a new variant of the FTTC method : the *projected FTTC method* (*p–FTTC*). This variant starts with a

classical FTTC method coupled with a Tikhonov regularization and ends by a projection step which ensures the localization condition.

Interpolation operator. As exposed in section 4.2, the DFT (i) requires to discretize the computational domain using an uniform and structured grid, and (ii) the knowledge of the beads displacement at every node in this grid. The role of the interpolation step is to estimate these new displacements, denoted by $\boldsymbol{u}_{\mathrm{g}}$, from the knowlegde of the experimental displacements $\boldsymbol{u}_{\mathrm{b}}$. This estimation is performed by using an interpolation operator which is a linear operator from $\mathbb{R}^{2N_{\mathrm{b}}}$ (N_{b} denoting the number of beads) into a specific functional space depending on the regularity imposed to the interpolant.

We used the *natural neighbor interpolation* (see [5] for a review of the main methods for solving the scattered data interpolation problem). This method gives a good balance between accuracy and computational time. The interpolant function $\boldsymbol{u}_{\mathrm{g}}$ can be written as the linear combination

$$\boldsymbol{u}_{\mathrm{g}} \,:\, \boldsymbol{x} \in \Omega \longmapsto \boldsymbol{u}_{\mathrm{g}}(\boldsymbol{x}) = \sum_{k=1}^{N_{\mathrm{b}}} \varphi_k(\boldsymbol{x})\, \boldsymbol{u}_{\mathrm{b},k} \in \mathbb{R}^2 \tag{36}$$

where $\varphi_k(\cdot)$ is the shape function associated with the k-th bead displacement $\boldsymbol{u}_{\mathrm{b},k}$. The shape functions have a compact support and are globally C^0 [23] (and even C^∞ except at beads locations). In the sequel, we denote by X_{g} the space of all functions of the form (36).

Tikhonov regularization of the unconstrained FTTC method. Schwarz *et al.* pointed out [22] that the TFM problem cannot be correctly solved with the BEM without using a regularization method. This observation was confirmed for the FTTC method [21]. Here, we derive a Tikhonov regularized FTTC method by using the framework developed in section 2.

The spaces are chosen as follows. Since we want to replace the data $\boldsymbol{u}_{\mathrm{b}}$ by its interpolant $\boldsymbol{u}_{\mathrm{g}}$ defined by (36), the space X_{b} must be replaced by X_{g}. So, we choose $V = X_{\mathrm{g}}$. On the other hand, we choose $H = \boldsymbol{L}^2(\Omega)$. We do not impose any biomechanical constraint, so $H_{\mathrm{c}} = H$. Note that since $X_{\mathrm{b}} = X_{\mathrm{g}}$ is then a finite dimensional space, we can simultaneously identify H and X_{b} with their respective dual spaces.

Under these conditions, both operators P_{c} and B involved in (17) reduce to the identity operator.

Then, we can rewrite the abstract equations (17) as the equation $A^{-\mathsf{T}}A^{-1}\boldsymbol{T}_\varepsilon + \varepsilon\,\boldsymbol{T}_\varepsilon = A^{-\mathsf{T}}\boldsymbol{u}_{\mathrm{b}}$. Taking into account the expression (28) of the operator A, this equation becomes $\mathbb{G}^{\mathsf{T}} * \mathbb{G} * \boldsymbol{T}_\varepsilon + \varepsilon\,\boldsymbol{T}_\varepsilon = \mathbb{G}^{\mathsf{T}} * \boldsymbol{u}_{\mathrm{b}}$ in the physical space and, thanks to the identity (31),

$$\widehat{\mathbb{G}}^{\mathsf{T}}(\boldsymbol{\xi})\,\widehat{\mathbb{G}}(\boldsymbol{\xi})\,\widehat{\boldsymbol{T}_\varepsilon}(\boldsymbol{\xi}) \;+\; \varepsilon\,\widehat{\boldsymbol{T}_\varepsilon}(\boldsymbol{\xi}) \;=\; \widehat{\mathbb{G}}^{\mathsf{T}}(\boldsymbol{\xi})\widehat{\boldsymbol{u}_{\mathrm{b}}}(\boldsymbol{\xi}) \qquad \text{for } \;\boldsymbol{\xi} \in \mathbb{R}^2 \tag{37}$$

in the Fourier space. This last equation appears as a regularized form of the normal equation related to $\widehat{\mathbb{G}}(\boldsymbol{\xi})\,\widehat{\boldsymbol{T}_\varepsilon}(\boldsymbol{\xi}) = \widehat{\boldsymbol{u}_{\mathrm{b}}}(\boldsymbol{\xi})$.

The p–FTTC method. The p–FTTC method improves the classical FTTC method by allowing to impose the localization constraint with a projection operator. It can be summarized as follows.

(1) Compute the interpolant $\boldsymbol{u}_{\mathrm{g}} \in X_{\mathrm{g}}$ of the experimental beads displacements $\boldsymbol{u}_{\mathrm{g}}$ in the physical space and approximate its Fourier transform $\widehat{\boldsymbol{u}_{\mathrm{g}}}$ using the DFT.
(2) For each $\boldsymbol{\xi_n} \neq 0$ describing the non-zero nodes of the discretization grid (33) in the Fourier space, compute $\widehat{\boldsymbol{T}_\varepsilon}(\boldsymbol{\xi_n})$ by solving equation (37) for $\boldsymbol{\xi} = \boldsymbol{\xi_n}$.
(3) Impose the zero total force constraint $\int_\Omega \boldsymbol{T}_\varepsilon \,\mathrm{d}\boldsymbol{x} = 0$ (over Ω, not over the cell domain Ω_{c}) in the Fourier space by setting $\widehat{\boldsymbol{T}_\varepsilon}(0) = 0$.
(4) Then, go back into the physical space $\boldsymbol{T}_\varepsilon = \mathcal{F}^{-1}\widehat{\boldsymbol{T}_\varepsilon}$ by using the inverse–DFT.

(5) Finally, impose the localization constraint $\mathrm{supp}\,(\boldsymbol{T}_\varepsilon) \subset \overline{\Omega_\mathrm{c}}$ by applying the projection operator P_cs defined by $P_\mathrm{cs}\,\boldsymbol{T} \,:\, \boldsymbol{x} \in \Omega \longmapsto (P_\mathrm{cs}\,\boldsymbol{T})\,(\boldsymbol{x}) = \chi_\mathrm{c}(\boldsymbol{x})\,\boldsymbol{T}(\boldsymbol{x}) \in \mathbb{R}^2$.

Note that the traction stress $\boldsymbol{T}_\varepsilon$ calculated by the previous algorithm does not belong to the space H_c defined in (24). In other words, $\boldsymbol{T}_\varepsilon$ satisfies the localization constraint ($\mathrm{supp}\,(\boldsymbol{T}) \subset \overline{\Omega_\mathrm{c}}$) but, in general, $\int_{\Omega_\mathrm{c}} \boldsymbol{T}_\varepsilon \,\mathrm{d}\boldsymbol{x} \neq 0$.

5. Numerical comparison of Adjoint and p–FTTC methods

In this last section, results from simulations obtained using the adjoint method and the p–FTTC method are discussed. A particular attention is paid to the choice of the regularization parameter.

Experimental data. Experiments involving GFP–transfected RT112 cells (from bladder epithelial tissues, rather low invasiveness degree) have been performed on Polyacrylamide gels with Young modulus $E = 10$ kPa and Poisson ratio $\nu = 1/2$. Measurements of fluorescent beads positions have been made using confocal microscopy and displacements were deduced using a technique previously described [3].

***L*–curve.** There exists several methods [14, 16, 26] to select a suitable value of the regularization parameter ε. This choice is a crucial step to yield an accurate approximation of the stress field. In order to avoid the use of any additional information (for example, error level in experimental data), we have chosen the *L–curve criterion* [15]. This method is based on a plot of the parametric curve of the stress norm $|\boldsymbol{T}_\varepsilon|_2$ versus the residual norm $\left|BA^{-1}\boldsymbol{T}_\varepsilon - \boldsymbol{u}_\mathrm{b}\right|_2$ for all $\varepsilon > 0$ ($|\boldsymbol{v}|_2$ denoting the euclidian norm of a discretization of $\boldsymbol{v}$). The *L*–curves constructed by the adjoint and p–FTTC methods can be seen in Fig. 3 below (in unusual linear scale).

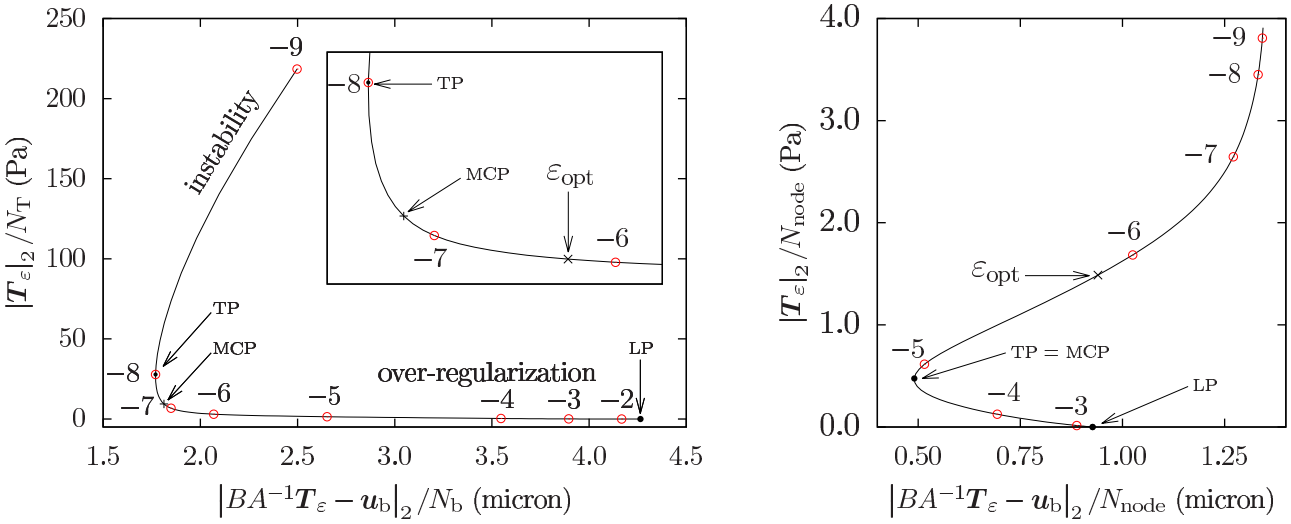

FIGURE 3. *L*–curves obtained using the adjoint method (left) and p–FTTC (right). Mechanical parameters : $E = 10$ kPa and $\nu = 1/2$. Data : $N_\mathrm{b} = 3\ 144$ beads. Mesh used by the adjoint method : 9 323 nodes, $N_\mathrm{T} = 1\ 109$ nodes in Ω_c and 18 332 triangles, P_1 interpolation. Spatial grid used by the p–FTTC method : 256×256 nodes ($N_\mathrm{node} = 65\ 536$), $N_\mathrm{T} = 6\ 396$ nodes in Ω_c. Some values of the decimal logarithm of ε are reported on the graphs (red circles). TP : turning point. MCP : maximum curvature point. LP : limit point. ε_opt : optimal value of the regularization parameter used in Fig. 4, 5 and 6.

The *L*–curve depicts the influence of the regularization parameter on the stress field. The one obtained with the adjoint method can be interpreted as follows. Low values of ε lead to high values of $|\boldsymbol{T}_\varepsilon|_2$. Indeed, when ε tends

to zero the regularization term vanishes in the Tikhonov functional (6) and then the stress field $\boldsymbol{T}_\varepsilon$ is strongly affected by the excitation of experimental errors in data. Next, the stability increases with the value of ε and the L–curve is decomposed into three regions. In the first one, $|\boldsymbol{T}_\varepsilon|_2$ and $\left|BA^{-1}\boldsymbol{T}_\varepsilon - \boldsymbol{u}_\mathrm{b}\right|_2$ decreases simultaneously until a *turning point* is reached. In the second region, just after this turning point, only $|\boldsymbol{T}_\varepsilon|_2$ decreases while $\left|BA^{-1}\boldsymbol{T}_\varepsilon - \boldsymbol{u}_\mathrm{b}\right|_2$ increases reasonably. In this region, the curvature is high and the point where the curvature is maximal is the *corner* of the L–curve. The third region is characterized by a low value of the curvature. In this region, $|\boldsymbol{T}_\varepsilon|_2$ decreases slowly and $\left|BA^{-1}\boldsymbol{T}_\varepsilon - \boldsymbol{u}_\mathrm{b}\right|_2$ increases steadily. This is due to the importance of the regularization term in the Tikhonov functional. Hence, in this region, the stress field is *over-regularized*. Finally, for high values of ε the Tikhonov functional is totally dominated by its regularization term, so $|\boldsymbol{T}_\varepsilon|_2$ tends to zero and the residual norm tends to $|\boldsymbol{u}_\mathrm{b}|_2$. Hence, the L–curve presents a limit point when ε tends to infinity.

The L–curve obtained with the p–FTTC method is somehow different, but turning point and its corner are even more evident, so that the regions identified in the previous L–curve can be identified.

Selection of the regularization parameters. In the region of higher curvature, the requirements of stability for $\boldsymbol{T}_\varepsilon$ and of the small value for the residual norm are well balanced. So, the value of ε corresponding to the corner of the L–curve is a natural candidate to give the optimal value of the regularization parameter [15]. We have checked this value, but, unfortunately, the corresponding stress field was unrealistic.

To find a better estimate of the stresses, we have used the following technique. We have visualized the stress vectors corresponding to a range of values of ε near to the corner of the L–curve. Initially, the stress vectors point in all directions, with a very irregular manner, then as ε is increased, a rearrangement of the vectors orientation takes place and these stresses directions become stable. As ε is further increased, the vector patterns remain stable in direction but their norms decrease. This last behavior corresponds to over-regularized solutions. Thus the optimum value of ε is chosen as the first value leading to a stabilized orientation for the directions of the stress vectors. This chosen value is found in the vicinity of the high curvature of the curve, but not necessarily at the highest local curvature. With the data and parameters used in Fig. 3, we have obtained $\varepsilon = 7.0 \times 10^{-6}$ in the case of the adjoint method and $\varepsilon = 1.5 \times 10^{-6}$ in the case of the p–FTTC method.

Comparison of the computed traction stresses. The estimated stress fields corresponding to these selected values of ε can be seen in Fig. 4 (stress vectors) and 5 (stress norm) below. These results seem in good agreement. But although the orders of magnitude are rather similar, some differences are however present. In particular

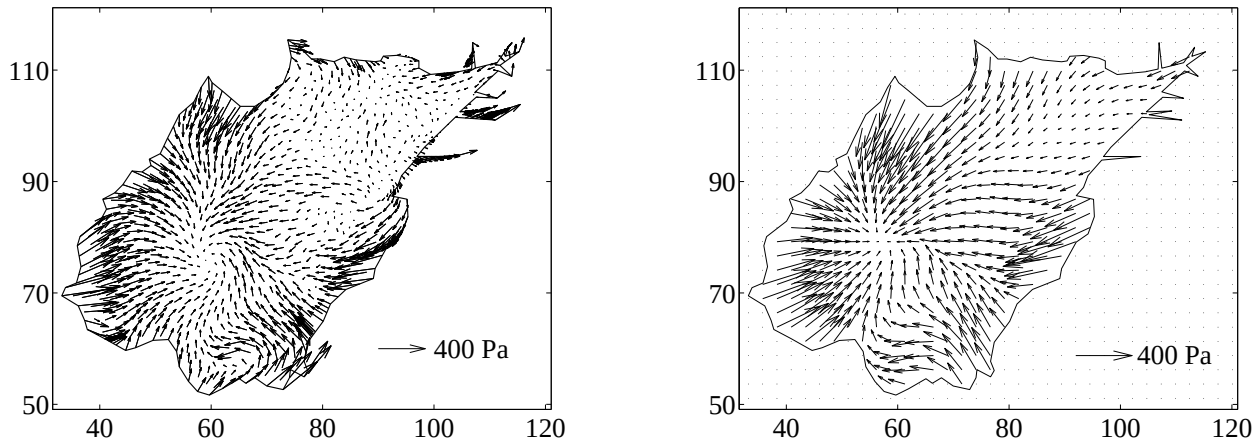

FIGURE 4. Stresses vectors obtained with the adjoint method (left) and the p–FTTC metod (right). The parameters have the same values as in Fig. 3. Regularizatioin parameter : $\varepsilon = 7 \times 10^{-7}$ for the adjoint method and $\varepsilon = 1.5 \times 10^{-6}$ for the p–FTTC method.

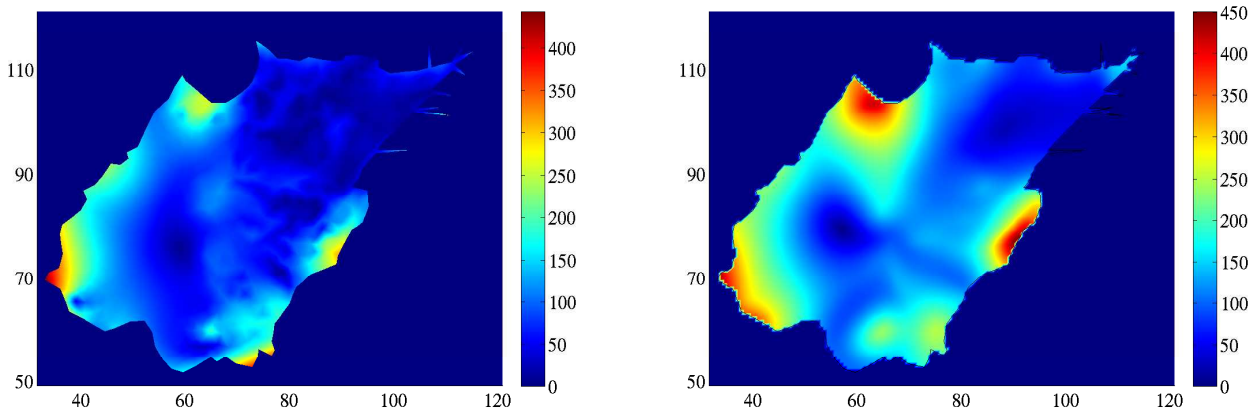

FIGURE 5. Stresses norms obtained with the adjoint method (left) and the p–FTTC metod (right). The parameters have the same values as in Fig. 4.

(i) the areas of the high stresses are different, (ii) different stress directions are found in the lower right and top parts of the cell. Moreover, as shown in Fig. 6, the adjoint method predicts non negligible stresses in filipodia (sharp shapes of the cell membrane) while the p–FTTC method does not that. Finally, the p–FTTC smoothes the stresses more than the adjoint method.

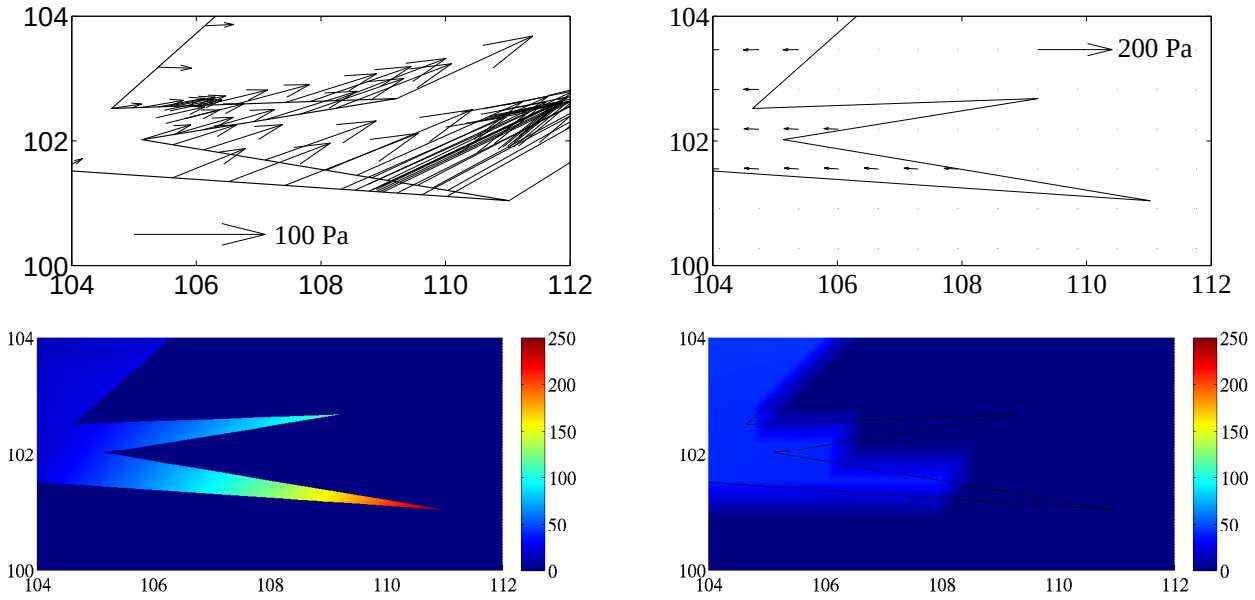

FIGURE 6. Stress field near a filipod obtained with the adjoint method (left) and the p–FTTC method (right). The parameters have the same values as in Fig. 3.

Conclusion. It can be concluded that the p–FTTC can be a good approximation of the solution but it has disadvantages as compared to the AM method. The p–FTTC method is in any case more accurate than the classical FTTC method [8], which does not ensure the biomechanical constraints of zero stresses outside the cell. Furthermore, the second condition (null sum of stresses) is also satisfied. As one wants to improve this

solution, it is better to use the AM method, in particular it enables to obtain local refinements of the solution in particular where filipodia are located. It is important to define stress directions precisely at these locations, whereas the p–FTTC method does not provide this information at all.

6. Conclusion

We have presented an abstract variational framework which allows to formulate the inverse problem of the TFM by combining contrained minimization theory with Tikhonov regularization. The biomechanical conditions satisfied by the cell are related to mathematical constraints and are imposed thanks to a projection operator. As specific applications, the adjoint and the FTTC methods can be derived in this framework by choosing suitable formulations for the direct problem. Furthermore, we have used the projection operator of the adjoint method to improve the FTTC method. This improvement imposes the zero traction stress condition outside the cell and it is achieved using the regularized FTTC method followed by a projection step. This improved FTTC, the so-called p–FTTC, yields acceptable results.

The numerical simulations have shown qualitative agreement between the adjoint and FTTC methods and have emphasized the choice of the value of the regularization parameter as the *critical step*. This choice was achieved by using the L–curve criterion in a semi-manual mode. But this issue requires further mathematical discussions and numerical experiments. In particular a test case is needed to definitely conclude on this choice and to compare the accuracy of both methods.

Références

[1] R. A. Adams and J. J.-F. Fournier. *Sobolev Spaces*, volume 140 of *Pure and applied mathematics*. Academic Press, New York, USA, 2003.

[2] D. Ambrosi. Cellular traction as an inverse problem. *SIAM J. Appl. Math.*, 66 :2049–2060, 2006.

[3] D. Ambrosi, A. Duperray, V. Peschetola, and C. Verdier. Traction patterns of tumor cells. *J. Math. Biol.*, 58 :163–181, 2009.

[4] N. Q. Balaban, U. S. Schwarz, D. Riveline, P. Goichberg, G. Tzur, I. Sabanay, D. Mahalu, S. Safran, A. Bershadsky, L. Addadi, and B. Geiger. Force and focal adhesion assembly : a close relationship studied using elastic micropatterned substrates. *Nat. Cell Biol.*, 3(5) :466–472, 2001.

[5] T. Bobach. *Natural Neighbor Interpolation - Critical Assessment and New Results*. PhD thesis, TU Kaiserslautern, 2008.

[6] A. Böttcher, B. Hofmann, U. Tautenhahn, and M. Yamamoto. Convergence rates for Tikhonov regularization from different kinds of smoothness conditions. *Applicable Analysis*, 85(5) :555–578, 2006.

[7] H. Brezis. *Functional Analysis, Sobolev Spaces and Partial Differential Equations*. Universitext. Springer verlag, New York, 2011.

[8] J. P. Butler, I. M. Tolic-Norrelykke, B. Fabry, and J. J. Fredberg. Traction fields, moments, and strain energy that cells exert on their surroundings. *Am. J. Physiol. Cell Physiol.*, 282(3) :C595–C605, 2002.

[9] P. G. Ciarlet. *Mathematical elasticity : Volume 1 Three-Dimensional Elasticity*, volume 20 of *Studies in Mathematics and its Applications*. North-Holland, Amsterdam, 1988.

[10] P. G. Ciarlet. *Introduction to linear numerical algebra and optimization*. Texts in Applied Mathematics. Cambridge University Press, Cambridge, 1989.

[11] M. Dembo and Y. L. Wang. Stresses at the cell-to-substrate interface during locomotion of fibroblasts. *Biophys. J.*, 76(4) :2307–2316, 1999.

[12] H. W. Engl, M. Hanke, and Neubauer N. *Regularization of Inverse Problems*, volume 375 of *Mathematics and its applications*. Kluwer Academic Publishers, Dardrecht, The Netherlands, 1996.

[13] M. Frigo and S. G. Johnson. The design and implementation of FFTW3. *Proceedings of the IEEE*, 93(2) :216–231, 2005. Special issue on "Program Generation, Optimization, and Platform Adaptation".

[14] P. C. Hansen. *Discrete Inverse Problems : Insight and Algorithms*. Fundamentals of Algorithms. SIAM Press, Philadelphia, PA, USA, 2010.

[15] P. C. Hansen and D. P. O'Leary. The use of the l-curve in the regularization of discrete ill-posed problems. *SIAM J. Sci. Comput.*, 14(6) :1487–1503, 1993.

[16] A. Kirsch. *An introduction to the mathematical theory of inverse problems*, volume 120 of *Applied Mathematical Sciences*. Springer verlag, New York, second edition, 2011.

[17] L. Landau and E. Lisfchitz. *Théorie de l'élasticité*. Editions Mir, 1967.

[18] J. L. Lions. *Optimal control of systems governed by partial differential equations*. Springer verlag, Berlin, 1971.
[19] R. Michel, V. Peschetola, B. Bedessem, J. Etienne, D. Ambrosi, A. Duperray, and C. Verdier. Inverse problems for the determination of traction forces by cells on a substrate : a comparison of two methods. *Comput Methods Biomech. Biomed. Eng.*, 15(S1) :27–29, 2012.
[20] V. Peschetola, V. Laurent, A. Duperray, R. Michel, D. Ambrosi, L. Preziosi, and C. Verdier. Time–dependent traction force microscopy for cancer cells as a measure of invasiveness. *Cytoskeleton*, 70(4) :201–214, 2013.
[21] B. Sabass, M. L. Gardel, C. M. Waterman, and U. S. Schwarz. High resolution traction force microscopy based on experimental and computational advances. *Biophys. J.*, 94(1) :207–220, 2008.
[22] U. S. Schwarz, N. Q. Balaban, D. Riveline, A. Bershadsky, B. Geiger, and S. A. Safran. Calculation of forces at focal adhesions from elastic substrate data : the effect of localized force and the need for regularization. *Biophys. J.*, 83(3) :1380–1394, 2002.
[23] N. Sukumar, B. Moran, A. Yu. Semenov, and Belikovm V. V. Natural neighbour galerkin methods. *Int. J. for Num. meth. Engineering*, 50(1) :1–27, 2001.
[24] H. Tanimoto and M. Sano. Dynamics of traction stress field during cell division. *Phys. Rev. Lett.*, 109 :248110, 2012.
[25] G. Vitale, D. Ambrosi, and L. Preziosi. Force traction microscopy : an inverse problem with pointwise observations. *J. Math. Anal. Appl.*, 395(2) :788–801, 2012.
[26] C. R. Vogel. *Computational methods for inverse problems*. Frontiers in Applied Mathematics. SIAM Press, Philadelphia, PA, USA, 2002.
[27] P. Witomski and C. Gasquet. *Fourier Analysis and Applications : Filtering, Numerical Computation, Wavelets*, volume 30 of *Text in Applied Mathematics*. Springer verlag, New York, 1999.